Solar Energy 288 (2025) 113263

Contents lists available at ScienceDirect

Solar Energy

journal homepage: www.elsevier.com/locate/solener

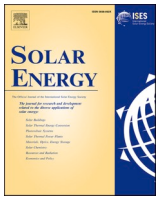

The influence of applying a solar dish to parallel-flow configurations of a Brayton cycle

C.C. Cockcroft, W.G. Le Roux *

Department of Mechanical and Aeronautical Engineering, University of Pretoria, Private Bag X20, Hatfield, Pretoria 0028, South Africa

ARTICLE INFO

Keywords:
Brayton cycle
Gas turbine
Turbocharger
Solar receiver
Concentrating solar power
Recuperation

ABSTRACT

When adding additional pressure loss components to a Brayton cycle, parallel-flow cycles can be a viable alternative for single-shaft and twin-shaft gas turbines. This study seeks to investigate how a solar heat input, captured via a solar dish and open-cavity tubular receiver, influences various simple and recuperated parallel-flow cycle configurations. Two solar receiver placements are considered: before the combustor, and before the power turbine (which is in parallel with the cycle). Various power turbine split-off points are considered: after the compressor, after the recuperator, after the solar receiver and after the combustor. In this work, various novel solar-dish parallel-flow Brayton cycles that make use of combinations of commercial radial turbochargers to form microturbine configurations are therefore investigated. The best-performing main shaft turbocharger, the G25-550 (AR = 0.92), was selected for analysis together with the GBC14-200 or the GBC17-250 as the power turbine. Variable recuperator dimensions were also introduced to obtain maximum fuel-based thermal efficiencies while remaining within, or as close as possible to, the maximum allowable gasifier turbine inlet temperatures. For unrecuperated cycles, the cycle with the solar receiver placed before the combustor and the power turbine split-off point directly after the combustor provided the best fuel-based thermal efficiency of 7 % at a pressure ratio of 2.75 (with 14.5 kW power output). For recuperated cycles, the cycle with a split-off point directly after the compressor, flowing to both the solar receiver and power turbine, achieved the highest fuel-based thermal efficiency of 22 % at a pressure ratio of 1.5 (with 3 kW power output).

1. Introduction

Access to electricity is a major factor in the welfare of communities, therefore, alternative power sources need to be considered in areas with insufficient power supply [1]. South Africa, and many other countries, face electricity supply issues. There have been many developments in systems capable of supplying electricity via renewable means, including through the use of concentrating solar power (CSP) [2]. CSP systems provide a viable clean and renewable electricity supply alternative, especially in areas with sunny and dry climates [3]. South Africa has an annual full day global horizontal irradiance average of 220 W/m^2, which far exceeds the 150 W/m^2 average for the USA and the 100 W/m^2 average for the UK [4]. Thus, South Africa has ample solar resources for the development of a competitive CSP industry, which also has global potential [5]. Solar radiation potential levels are also high in Asia (particularly in India), Southern Europe, South America, Australia, and Africa [6].

A recuperated solar-dish Brayton cycle has been modelled in various studies at the University of Pretoria to show the value of a small-scale CSP cycle. Refs. [7–9] optimised solar receiver and recuperator geometries via entropy generation minimisation. Le Roux [10] analysed the cycle as a hybrid cycle that utilises the combustion of liquified petroleum gas (LPG) along with a solar heat input. The study considered cogeneration via heating water and electricity generation. It was determined that an energy utilisation factor (EUF) of at least 52 % is needed for the hybrid cycle to form a competitive alternative to South Africa's power grid [10]. Le Roux & Sciacovelli [11] further expanded this cycle through considering different recuperator dimensions and different metallic phase-change materials integrated within the solar receiver for short-term thermal energy storage options. Roosendaal et al. [12] investigated an alternative to the cycle's concentrator to reduce the expenses associated with developing a highly optically accurate solar dish. Humbert et al. [13] developed and tested an experimental model of a latent heat thermal energy storage unit allowing for a thermal storage of up to 17.5 kWh after 10 h of charging. This showed feasible increases in the solar utilisation factor of the cycle.

Swanepoel et al. [14] implemented and tested a full-scale prototype,

* Corresponding author.
E-mail address: willem.leroux@up.ac.za (W.G. Le Roux).

https://doi.org/10.1016/j.solener.2025.113263
Received 15 October 2024; Received in revised form 17 December 2024; Accepted 7 January 2025
Available online 22 January 2025

Nomenclature

Symbols

A	Area [m^2]
a	Recuperator channel width or receiver aperture side length [m]
b	Recuperator channel height [m]
d	Tube diameter [m]
F	View factor
f	Friction factor
H	Height [m]
h	Specific enthalpy [J/kg]
K	Loss coefficient
k	Thermal conductivity [W/mK]
L	Length [m]
$\dot{m}$	Mass flow rate [kg/s]
N	Number of tube sections
P	Pressure [Pa]
$\dot{Q}$	Heat transfer rate [W]
T	Temperature [K]
t	Thickness [m]
$\dot{W}$	Rate of work [W]

Greek symbols

ε	Emissivity
η	Efficiency
λ	Heat transfer coefficient [W/m^2K]
σ	Stefan-Boltzmann constant [W/m^2K]

Subscripts

0	Ambient
1–8	States 1–8
AF	Actual flow
CC	Combustion chamber
CF	Corrected flow
comp	Compressor
cond	Conduction
conv	Convection
fuel	Fuel-based
gt	Gas turbine
in	Inlet
ins	Insulation
loss	Loss
n	Tube section number
net	Net amount
o	Outer
out	Outlet
pt	Power turbine
rad	Radiation
rec	Recuperator
SR	Solar receiver
s	Surface
th	Thermal
y	Elbow number

Superscripts

*	Solar

Abbreviations

AR	Aspect Ratio
CC	Combustion Chamber
CSP	Concentrating Solar Power
EUF	Energy Utilisation Factor
G	Generator
GT	Gasifier Turbine
HTT	High-Temperature Turbine
ITT	Intermediate-Temperature Turbine
ITT(S)	Intermediate-Temperature Turbine (Solarised)
LPG	Liquefied Petroleum Gas
LTT	Low-Temperature Turbine
NTU	Number of Transfer Units
OMSoP	European Optimised Microturbine Solar Power system
PT	Power Turbine
SR	Solar Receiver
SR-CC	Solar receiver placement 1 (before the *CC*)
SR-PT	Solar receiver placement 2 (before the *PT*)
ST-CHP	Solar Turbo-Combined Heat and Power
TIAC	Turbine Inlet Air Cooling

as part of the ST-CHP project funded by Innovate UK, with a combustion chamber, a helically coiled solar receiver, a latent heat thermal energy storage unit, and a Samad Power [15] micro gas turbine. The study found that high pressure losses in the combustion chamber (due to high combustion chamber inlet temperatures), solar receiver, recuperator, and piping components resulted in the micro gas turbine not producing sufficient power to allow for advances via solar heat and recuperation [14]. To quantify this, a late afternoon test of the hybrid prototype was able to generate a peak power output of 0.4 kWe, which stabilised to 0.145 kWe [14]. When this prototype was tested without solar hybridisation or recuperation, the prototype was able to generate 1.05 kWe of power output [14]. Thus, pressure losses form a challenge in single-shaft solar-dish Brayton cycles. Further ongoing developments at the University of Pretoria consist of deploying a mobile unit, similar to the unit by Swanepoel et al. [14]. The mobile unit excludes a recuperator and uses low-cost vacuum control systems, for each individual solar facet that forms a bigger solar-dish, as was done in the study by McGee et al. [16]. These control systems serve the purpose of allowing for individual focal length variation in each facet to improve the optical focus of the dish system via individual membrane depth adjustment.

The oldest full-scale solar-dish Brayton cycle was implemented between 1982 and 1984 by Garret AiResearch and Sanders Associates [17–19]. This cycle produced a power output of 0.4 kWe for a 44 m^2 solar dish and a power output of 2.9 kWe for a 49 m^2 gas-solar dish hybrid. Lanchi et al. [20] presented experimental development for the OMSoP solar-dish Brayton cycle project. Aichmayer et al. [21] developed a model for scaling up the receiver in a solar-dish Brayton cycle. Wang et al. [22] investigated overheating protection strategies for components in the OMSoP project for operation at high solar irradiation levels. Aichmayer et al. [23] have done a receiver design analysis for the OMSoP project to ensure that the receiver components maintain their integrity for a wide range of operational conditions. A transient OMSoP system model was developed to optimise the efficiency of the system with a targeted average thermal efficiency of 21 % and an expected power output of 10 kWe [24], however, this has not yet been experimentally proven. The SolarCAT project [25] is another Brayton cycle CSP project, however, this project has not progressed beyond initial experimental subassembly testing.

Considering Refs. [1,7–13] and [15–25], extensive research has been conducted for implementing a CSP system in South Africa using single-shaft gas turbine layouts. There is a global shift towards increasing the utilisation of solar energy as a viable electricity generation alternative [26], thus research towards developing a CSP system has global reach. Additionally, it is feasible to use commercial turbochargers as the cycle microturbine due to the high importation and taxation rates associated with sourcing microturbines in countries such as South Africa [27]. This

feasibility is shown in the studies by Le Roux et al. [7], Le Roux & Meyer [9], Le Roux [9], Le Roux & Sciacovelli [11], De Beer et al. [28], and Van der Merwe et al. [27]. Visser et al. [29] have developed a commercial gas turbine product using an off-the-shelf automotive turbocharger in a small-scale combined heat and power (CHP) system, further showing the feasibility of using automotive turbochargers in gas turbine cycles.

For the studies by Refs. [14] and [17–25], cycle pressure losses result in low to no power output results, reducing the success of the single-shaft gas turbine cycles. Van der Merwe et al. [27] introduced parallel-flow configurations as an alternative. The advantage of parallel-flow cycles is that the influence of pressure-drop can be negated by placing the power turbine split-off point prior to some of the pressure loss processes [27]. This is feasible for cycles with recuperators and solar receivers, as these components are added to improve cycle thermal efficiency, but add pressure losses to the cycle. Pressure losses result in a lower pressure ratio over the turbine which reduces the power generation potential of the cycles. Cockcroft & Le Roux [30,31] expanded upon the parallel-flow cycle concept. Cockcroft & Le Roux [30] investigated turbine inlet air cooling, through cooling the compressor inlet, in a simple parallel-flow cycle. This study showed that turbine inlet air cooling only improves cycle performance through extending the operational pressure ratio range of the cycle. Cockcroft & Le Roux [31] investigated recuperated parallel-flow cycles with different flat-plate recuperator dimensions, and showed that recuperation greatly improves thermal efficiency with maximum unrecuperated and recuperated cycle thermal efficiencies of 3.02 % and 19.2 %, respectively.

The objective of the study by Cockcroft & Le Roux [31] was to determine the influence of applying a recuperator, defined in terms of flat-plate recuperator geometry, on various simple parallel-flow cycles. Additionally, the study introduced and analysed the intermediate-temperature turbine (ITT) cycle as a novel cycle concept in which the parallel-flow split-off point is placed between the recuperator cold-side outlet and the combustion chamber inlet. The current study further expands on this concept through adding a solar receiver to the simple and recuperated parallel-flow cycles. Thus, the scope of the current study involves an investigation into how a solar heat input, using an open-cavity tubular receiver (optimised in the study by Ref. [8]) with a fixed solar dish diameter of 4.8 m, affects the results of a parallel-flow gas turbine cycle developed from turbochargers. Different possible placements of a solar receiver in various simple and recuperated parallel-flow cycles are considered to establish which parallel-flow configuration and solar receiver placement allows for the best fuel-based thermal efficiency, while maintaining an acceptable turbine inlet temperature.

2. Methodology

For an analytical investigation regarding applying solar heat inputs to a parallel-flow Brayton cycle, the cycle layouts and cycle components are defined. Hereafter, the solution procedures for solving each cycle case are discussed. Note that the simple LTT model has been verified in the study by Cockroft & Le Roux [30] and the simple and recuperated cycle methodologies have been detailed in the studies by Cockcroft & Le Roux [30,31]. Thus, the current section seeks to summarise the modelling procedures with the reference studies being available for further information regarding modelling procedures. The current study adds recuperation and the application of CSP via an open-cavity tubular receiver to the verified cycle study. For this the solar receiver model is verified in Appendix A and the same recuperation model is used as in the study by Cockcroft & Le Roux [31].

2.1. Cycle layouts

This study makes use of two different types of solar cycles, a simple solar cycle and a recuperated solar cycle. Each of these solar cycle types are split into various configurations based on the power turbine split-off point together with various options for the placement of the solar receiver. The different solar receiver placements are split into two options: solar receiver placement 1, for the placement of the solar receiver prior to the combustion chamber inlet; and solar receiver placement 2, for the placement of the solar receiver prior to the power turbine inlet.

The low-temperature turbine (LTT) cycle makes use of a split-off point directly after the compressor exit and the high-temperature turbine (HTT) cycle makes use of a split-off point directly after the combustion chamber outlet, as defined by Van der Merwe et al. [27]. The intermediate-temperature turbine (ITT) cycle is defined as a cycle wherein the cycle split-off point occurs directly after the cold-side exit of the recuperator. The placement of a solar receiver directly before the combustion chamber inlet, allows for a fourth split-off point option. This new split-off point option is termed the solarised intermediate-temperature turbine cycle – the ITT(S) cycle – wherein the split-off point occurs directly after the solar receiver outlet. This cycle can only exist when the receiver is incorporated into the cycle. In the recuperated solar cycle, which is still to be discussed, the recuperator is placed before the solar receiver. This means that when comparing the recuperated solar ITT cycle to the recuperated solar ITT(S) cycle, the ITT cycle split-off point is placed before the solar heating and is thus expected to have a lower split-off point temperature.

Furthermore, the non-solar cycles have been analysed in a previous study by Cockcroft & Le Roux [31] and follow the same layout and procedures as the cycle setups introduced in this study with the omittance of the solar receivers in the discussed layouts. Additionally, due to the parallel-flow operation of the cycle, the power generated through the expansion process in the gasifier turbine needs to equate to the power required to operate the compression process in the compressor [27]. This means that the power output of each cycle is equal to the power generated in the power turbine expansion process as per Eq. (1). The total thermal efficiency, η_{th}, of each cycle is then determined based on the ratio between the power output and the required cycle heat, as shown in Eq. (2). However, Eq. (3) is used to determine the fuel-based thermal efficiency of the cycle, as a better representation of the cycle performance. This fuel-based thermal efficiency better indicates how the addition of a solar receiver in the cycle can lessen the requirement for the injection of fuel into the cycle. The fuel-based thermal efficiency is expected to be higher than the total thermal efficiency due to not including the solar heat input in the equation. Note that for non-solar cycles, the total thermal efficiency and the fuel-based thermal efficiency equations are the same.

$$\dot{W}_{net} = \dot{W}_{gt} + \dot{W}_{pt} - \dot{W}_{comp} = \dot{W}_{pt} \tag{1}$$

$$\eta_{th} = \frac{\dot{W}_{net}}{\dot{Q}_{CC} + \dot{Q}_{SR}} \tag{2}$$

$$\eta_{fuel,th} = \frac{\dot{W}_{net}}{\dot{Q}_{CC}} \tag{3}$$

2.1.1. Simple solar cycle layouts: Receiver placement 1 (before the combustion chamber)

For the placement of the solar receiver prior to the combustion chamber, the cycle operates via the intake of ambient air at state 1, hereafter the ambient air undergoes a compression process that finalises at state 2. The air then enters the solar receiver. The solar receiver utilises solar energy from the solar dish to heat the air to state 3. This air enters the combustion chamber whereupon this air mixes with the LPG that is injected into the cycle to allow for combustion and a subsequent temperature increase at state 4. It is required that this combustion exit temperature, and the combined air–fuel mass flow rate allow for the power generated in the gasifier turbine to equate to the power required for the operation of the compressor, in the compression process from state 1 to state 2. This balance considers the effect that the pressure losses in the solar receiver and in the combustion chamber have on the

pressure ratio through the gasifier turbine. The net power output of the cycle is thus considered to be the power generated via the expansion process in the power turbine, that finalises at state 6. The exhaust pressures at states 5 and 6 equate to the ambient pressure which is why the pressure losses in the solar receiver and in the combustion chamber need to be considered for the determination of the pressure ratio through the gasifier turbine.

Fig. 1 shows that there are three possible parallel-flow split-off points for three possible parallel-flow simple solar cycle configurations when the first receiver placement is utilised. The first simple solar cycle is the simple solar LTT configuration, wherein the split-off point occurs directly after the compressor outlet at state 2, and thus the power turbine pressure ratio is not influenced by the pressure losses in the solar receiver nor in the combustion chamber. The second simple solar cycle is the simple solar ITT(S) cycle, wherein the split-off point occurs directly after the solar receiver outlet at state 3, and thus the power turbine pressure ratio is influenced only by the pressure losses in the solar receiver and not by the pressure losses in the combustion chamber. The third simple solar cycle is the simple solar HTT configuration, wherein the split-off point occurs directly after the combustion chamber outlet at state 4, and thus the power turbine pressure ratio is influenced by the pressure losses in both the solar receiver and in the combustion chamber.

2.1.2. Simple solar cycle layouts: Receiver placement 2 (before the power turbine)

For receiver placement 2, the cycle follows a similar operational procedure as in the first receiver placement, except the solar receiver heating process is shifted prior to the power turbine inlet. For this receiver placement, there are only two possible cycle split-off points, as shown in Fig. 2. The first simple solar cycle configuration is the simple solar LTT configuration, wherein the split-off point occurs directly after the compressor outlet at state 2, and thus the power turbine pressure ratio is not influenced by the combustion chamber pressure loss. The second simple solar cycle configuration is the simple solar HTT, and thus the power turbine pressure ratio is influenced by the combustion chamber pressure loss. The solar receiver heating process occurs prior to the power turbine inlet, at state 5, and thus the power turbine pressure ratio is influenced by the solar receiver pressure losses in both configurations.

2.1.3. Recuperated solar cycle layouts: Receiver placement 1 (before the combustion chamber)

For the recuperated solar cycle layouts, the various cycle configurations for the first dish placement are illustrated in Fig. 3. These various cycle configurations follow a similar base structure to the simple solar cycle layouts but with the inclusion of a recuperator to utilise the waste heat exiting the gasifier turbine. As in the solar cycle, the compression process operates on the intake of ambient air from state 1 to 2. The recuperator is placed with its cold-side process occurring between state 2 and 3. The cold-side of the recuperator is heated by the hot-side recuperation process occurring from state 6 to state 7 for the first receiver placement and from state 5 to state 6 for the second receiver placement.

In Fig. 3, the cycle split-off point can occur at different cycle states to form the recuperated solar LTT layout, the solar ITT layout, the solar ITT (S) layout, or the recuperated solar HTT layout. For the recuperated solar LTT layout, the split-off point occurs at the compressor outlet, at state 2, and thus the power turbine pressure ratio is not influenced by any of the pressure losses components. For the recuperated solar ITT

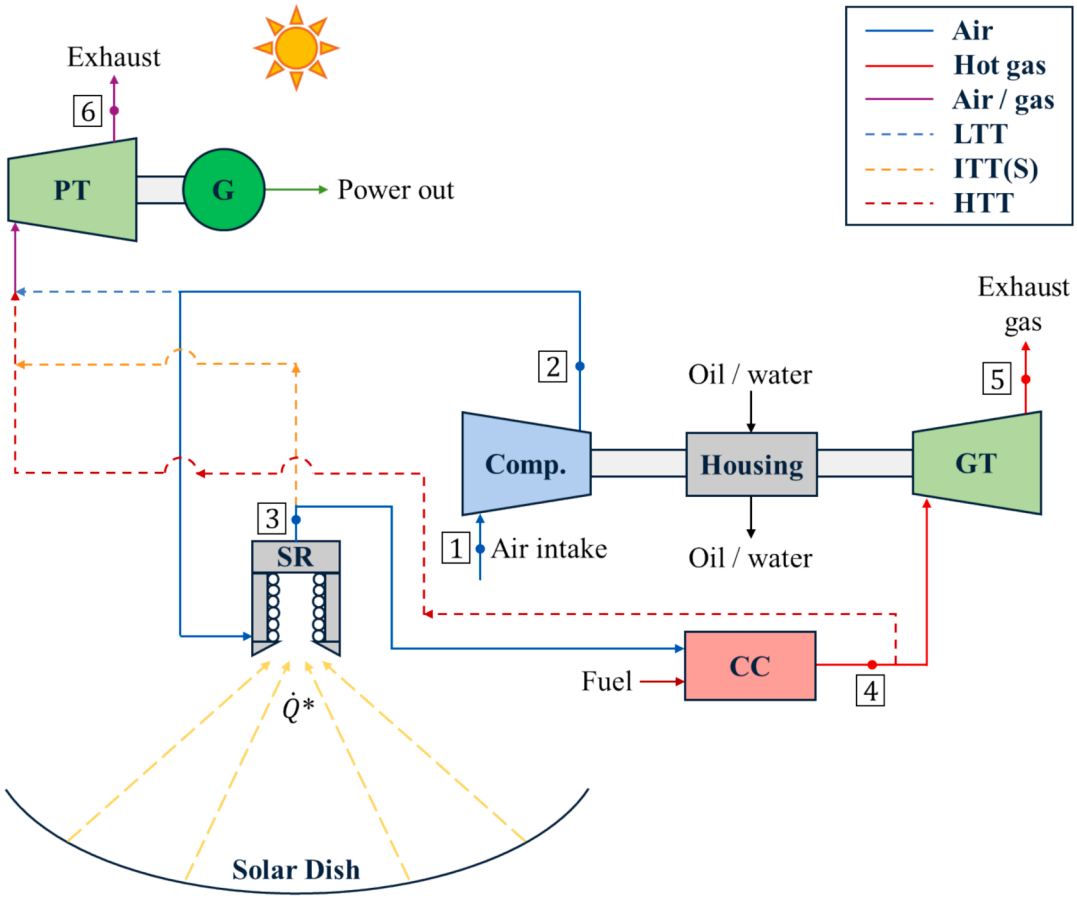

Fig. 1. Various simple solar parallel-flow configurations for solar receiver placement 1 (solar receiver before combustion chamber).

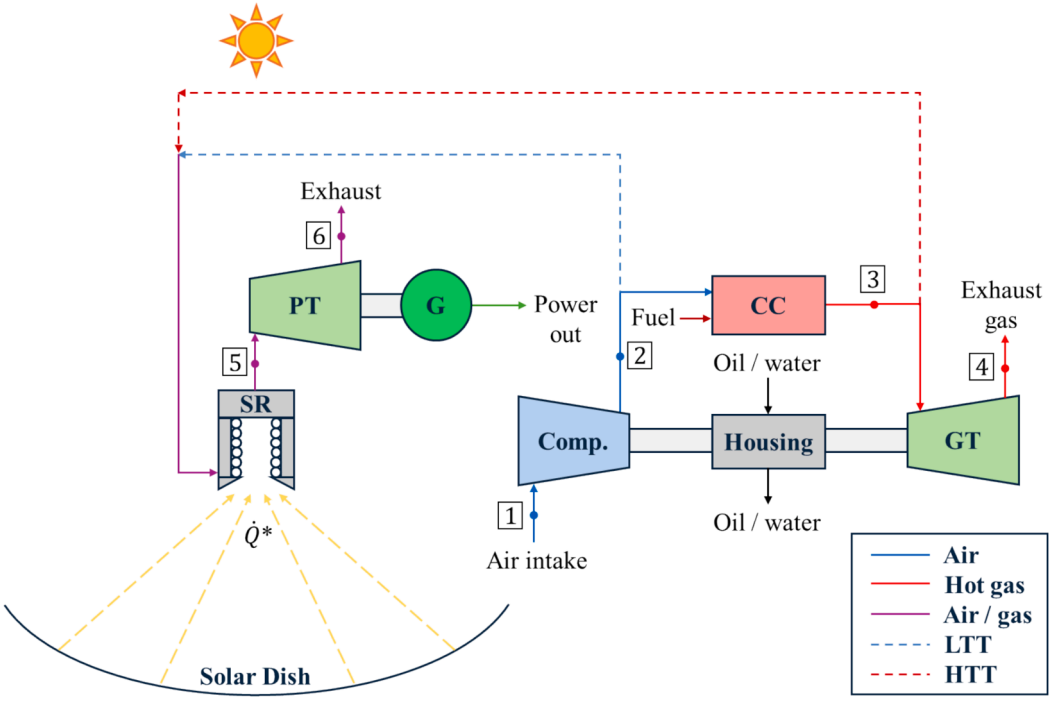

Fig. 2. Various simple solar parallel-flow configurations for solar receiver placement 2 (solar receiver before power turbine).

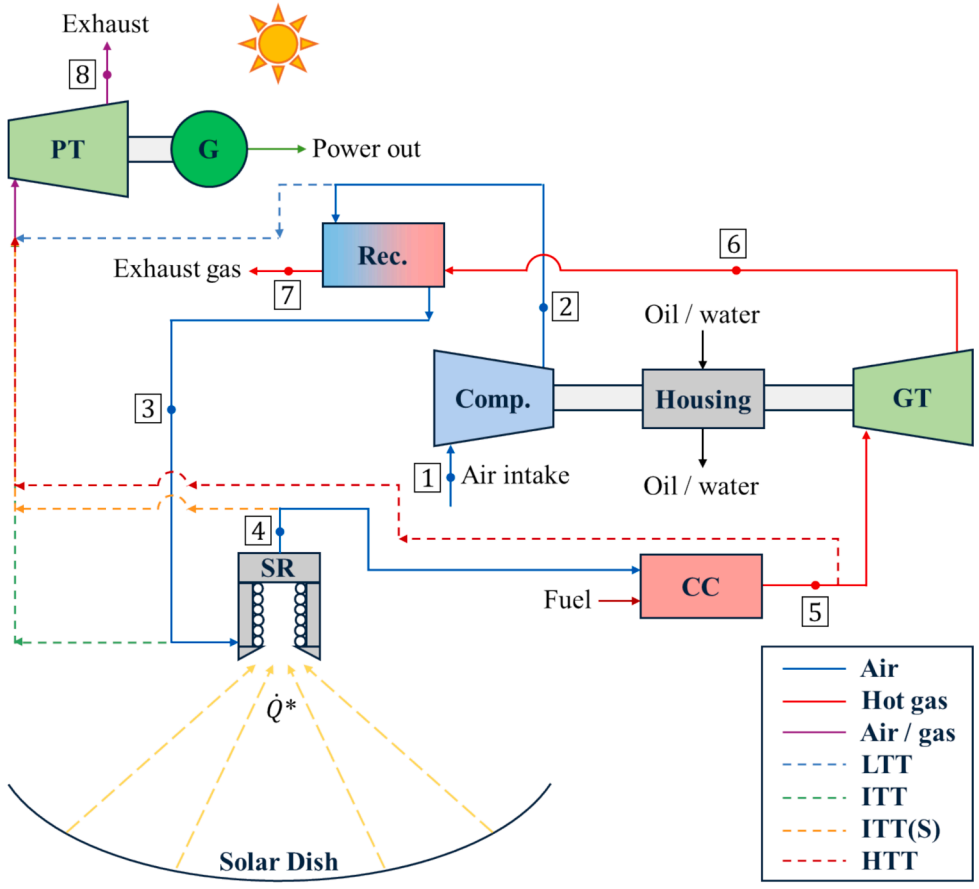

Fig. 3. Various recuperated solar parallel-flow configurations for solar receiver placement 1 (solar receiver before combustion chamber).

layout, the split-off point occurs at the cold-side outlet of the receiver outlet, at state 3, and thus the power turbine pressure ratio is influenced only by the pressure losses experienced by the cold-side of the recuperator. For the recuperated solar ITT(S) layout, the split-off point occurs at the solar receiver outlet, at state 4, and thus the power turbine pressure ratio is influenced by the pressure losses occurring in the cold-side of the recuperator and by the solar receiver pressure losses. Lastly, for the recuperated solar HTT layout, the split-off point occurs at the combustion chamber outlet, at state 5, and thus the power turbine pressure ratio is influenced by all the pressure loss components.

2.1.4. Recuperated solar cycle layouts: Receiver placement 2 (before the power turbine)

For the recuperated solar cycle layouts that make use of the second receiver placement, Fig. 4 shows that there are three possible parallel-flow configurations. These configurations are for the recuperated solar LTT, the recuperated solar ITT, and the recuperated solar HTT. The process flow and parallel-flow configurations follow the same general layouts and split-off placements as the recuperated layouts by Cockcroft & Le Roux [31]. Thus, each configuration's power turbine pressure ratio is influenced by the solar receiver pressure losses.

2.2. Component analysis

To analyse the introduced cycle configurations, the processes that occur throughout the cycles need to be detailed. This involves a characterisation of the compressor, gasifier turbine, power turbine, combustion chamber, recuperator, solar receiver, and the cycle exhaust to ambient conditions. The properties pertaining to the analysis of these processes are defined based on properties from CoolProp [32], with these properties being updated based on the reference properties as per Borgnakke & Sonntag [33]. The required material properties to define the structural basis of the recuperator and solar receiver are based on properties from Çengel & Ghajar [34]. Additionally, the cycles operate through the intake of ambient air and exhaust at ambient pressure. This ambient air is assumed to be at 300 K and with an atmospheric pressure of 86.6 kPa, as per the ambient air conditions in Pretoria, South Africa [7]. In addition to this, a wind speed of 2.5 m/s is considered for heat loss analyses [8].

2.2.1. Compressor and turbines

Automotive *Garrett Motion* [35] turbochargers are used to represent the compressor, gasifier turbine, and power turbine in this study. For this, the compressor and gasifier turbine are considered as a coupled off-the-shelf turbocharger and the power turbine operates via a separate shaft as per the turbocharger modelling procedures in Ref. [27]. To model these components, *Webplotdigitizer* [36] is used to convert the turbomachinery flow maps into a digital set of data that can easily be interpolated from for various design points in the cycle analyses. This digitised data is interpolated using contour plotting in Python. The resultant turbomachinery solving solution procedure is followed as per Ref. [30] with the mass flow rates being corrected for in terms of

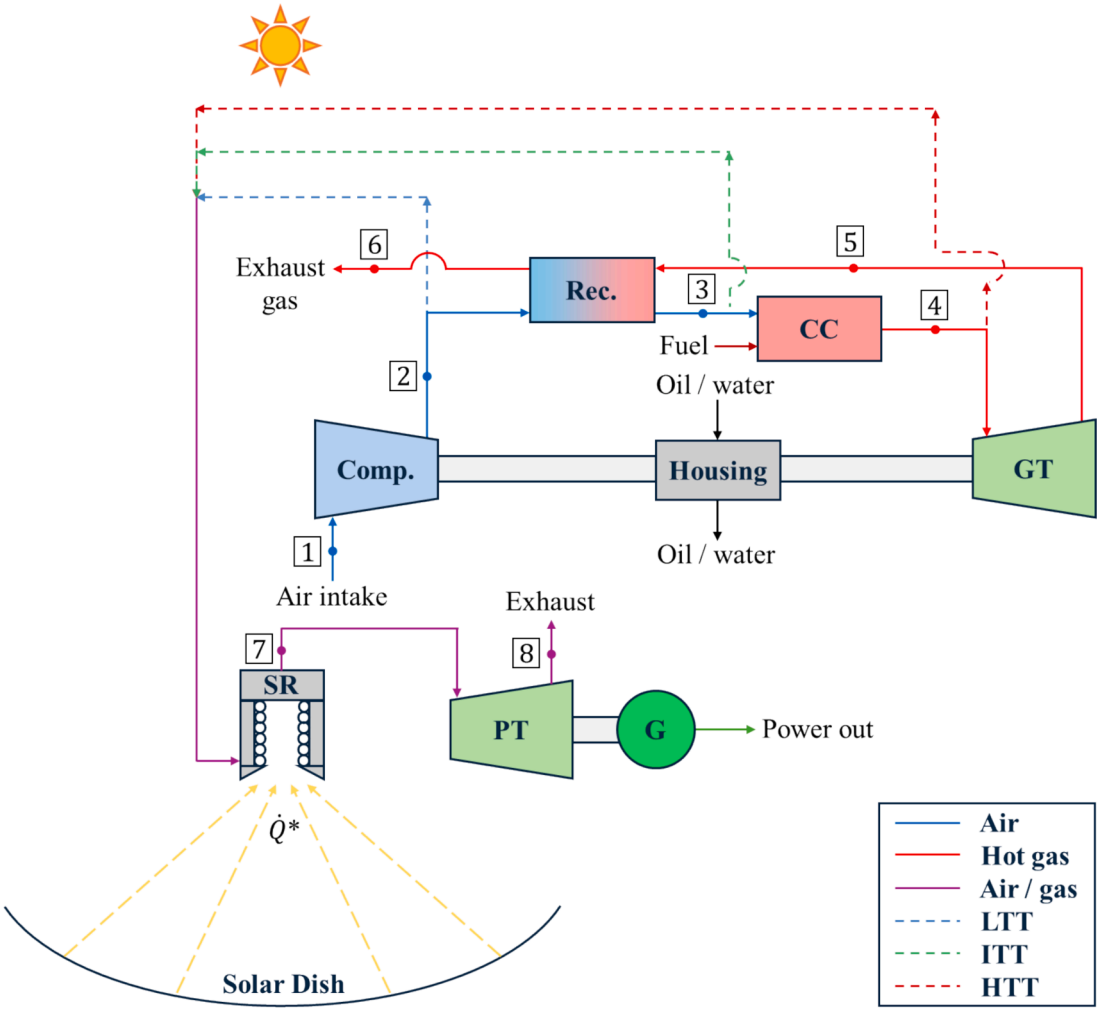

Fig. 4. Various recuperated solar parallel-flow configurations for solar receiver placement 2 (solar receiver before power turbine).

representing the ambient conditions in Pretoria, South Africa, from the turbomachinery flow maps via Eq. (4) and Eq. (5). CoolProp [32] is then used to determine the state properties associated with the relative states of the working fluid through the compressor, gasifier turbine, and power turbine.

$$\dot{m}_{comp,AF} = \frac{\left(\dot{m}_{gt,CF} - \dot{m}_{LPG} + \dot{m}_{pt}\right)\left(\frac{P_{gt,in}}{14.7\times6894.8}\right)}{\sqrt{\frac{\left(\left(T_{gt,in}-273.15\right)\times1.8+492\right)}{519}}} \tag{4}$$

$$\dot{m}_{comp,CF} = \dot{m}_{comp,AF}\frac{\sqrt{\frac{\left(\left(T_{comp,in}-273.15\right)\times1.8+492\right)}{545}}}{\left(\frac{P_{comp,in}}{13.95\times6894.8}\right)} \tag{5}$$

As a result of using commercial *Garrett Motion* turbomachinery, there is a restriction on the inlet temperature of the gas entering the turbines, with this limit being especially important in the modelling of the gasifier turbine inlet as the highest expected temperature state in the cycles. This limit is that the turbine inlet temperature may not exceed 1223 K (950 °C) [37], with the subsequent maximum allowable gasifier turbine inlet temperature being limited to no more than 1200 K to remain conservatively within the allowable limit.

2.2.2. Combustion chamber

For the combustion process, LPG is injected in the combustion chamber to combust with the portion of air that is not undergoing the power generation process in the power turbine. The standard composition of LPG in South Africa is used to model the fuel consisting of a composition that is 60 % propane and 40 % butane [38]. This chemical reaction is modelled via the principles of solving for the adiabatic flame temperature of the combustion process [33]. This temperature is modelled to equate the required gasifier turbine inlet temperature to balance the compressor and gasifier turbine work rates.

Considering that the air entering the combustion chamber is in excess, the subsequent required fuel mass flow rate is determined from the molar ratio of the process and through the relationship between the molar air–fuel ratio and the air–fuel ratio on a mass basis. Thus, the required outlet temperature of the combustion chamber and the required fuel flow are iteratively solved. This is done to make sure that the inlet temperature to the gasifier turbine and the mass flow rate through the gasifier turbine allows for the same rate of power generation that is required to operate the compressor. This is based on a fixed proportion of air, at a fixed temperature, entering the combustion chamber per iteration of the complete gas turbine cycle solution procedure. The values associated with this iterative process differ for each simulated pressure ratio and these values depend on the mass flow rates obtained from the turbomachinery flow maps (detailed in section 2.2.1). Note that this process is different to a traditional single-shaft cycle where the inlet temperature to the gasifier turbine can be changed to achieve different power output results. The reason for this difference is that in a parallel-flow cycle, the exact turbine inlet temperature needs to be solved for to equate the compressor and gasifier turbine work rates. The combustion process is discussed in detail in Ref. [31], for reference.

The relationship between the cycle mass flow rates and the heat generated in the combustion chamber is determined based on the control volume in Fig. 5. This results in a mass balance relation as per Eq. (6) and an associated combustion heat value determined via Eq. (7) [31].

$$\dot{m}_{gt} = \dot{m}_{comp} - \dot{m}_{pt} + \dot{m}_{LPG} \tag{6}$$

$$\dot{Q}_{CC} = \dot{m}_{gt}h_{CC,out} - \left(\dot{m}_{gt} - \dot{m}_{LPG}\right)h_{CC,in} - \dot{m}_{LPG}h_{LPG,in} \tag{7}$$

According to Lefebvre & Ballal [39], when an annular or annular-tube combustion chamber is used, the combustion chamber's pressure loss is expected to be approximately 6 %. This is the value used for the pressure loss in the combustion chamber in this study and thus results in the outlet pressure of the combustion chamber to be calculated as per Eq. (8) [31].

$$P_{CC,out} = (1 - 0.06)P_{CC,in} \tag{8}$$

2.2.3. Recuperator

The recuperated configurations make use of a recuperator with the same setup and analysis as in the recuperated cycle by Le Roux & Sciacovelli [11]. The reference study's recuperator is defined in terms of the geometry of a flat-plate recuperator and follows the modelling procedure developed by Nellis & Pfotenhauer [40] through the use of the effectiveness-NTU method for solving for the operation of a heat exchanger with heat loss considerations.

The geometry-modelled recuperator is shown in Fig. 6 and has defined geometry in terms of the recuperator length, L_{rec}, the recuperator width, a, the recuperator channel height, b, and the number of recuperator flow channels in a single direction, n. The number of recuperator channels has not been indicated in Fig. 6 but through a consideration of the recuperator channel height, the number of recuperator channels and the thickness of the recuperator plates, t, the recuperator height, H, can be determined. The recuperator plate thickness is 0.5 mm in this study so as to minimise the thermal resistance offered by the plates for adequate heat transfer while maintaining a sturdy design [11]. The material and insulation properties pertaining to the recuperator are based on theory by Çengel & Ghajar [34]. Furthermore, in the cycle analyses, the recuperator length and width are kept constant to lessen computational requirements. These constant values are based on the best-case geometries in the study by Le Roux & Sciacovelli [11] and thus the recuperator channel length and width are constant at 1.5 m and 0.225 m, respectively. This implies that the only recuperator variables that are investigated in terms of their influence on the cycle results are the channel height, b, and the number of channels, n.

2.2.4. Solar receiver

The solar receiver model is adapted from Ref. [8] and thus all geometries are kept constant based on the rectangular open-cavity tubular solar receiver model in Fig. 7. Note that the last three coils from the reference study have been removed to lessen the pressure drop through the receiver. The receiver geometries consist of a receiver side length of $a = 0.25$ m (for an aperture area of 0.625 m^2) and a depth of $2a$, with the cycle air flowing through six stainless-steel coils with a total length of 8 m and a tube diameter of 0.0833 m as per the optimisation procedure by Le Roux et al. [8].

The solar receiver functions using solar irradiation that is reflected

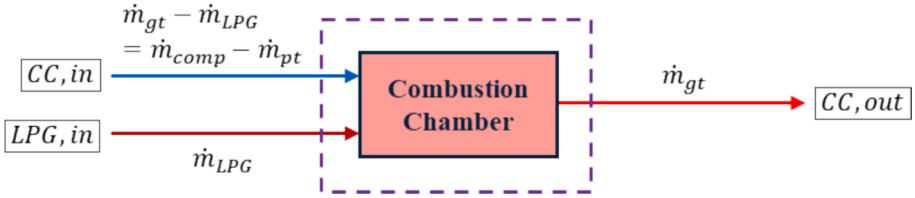

Fig. 5. Control volume analysis of the combustion chamber [31].

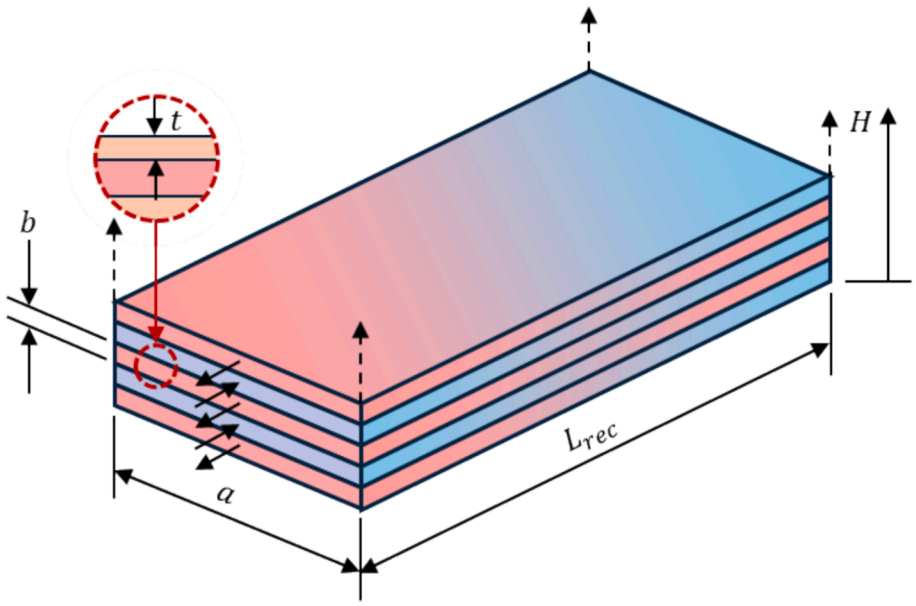

Fig. 6. Recuperator geometry and dimensions.

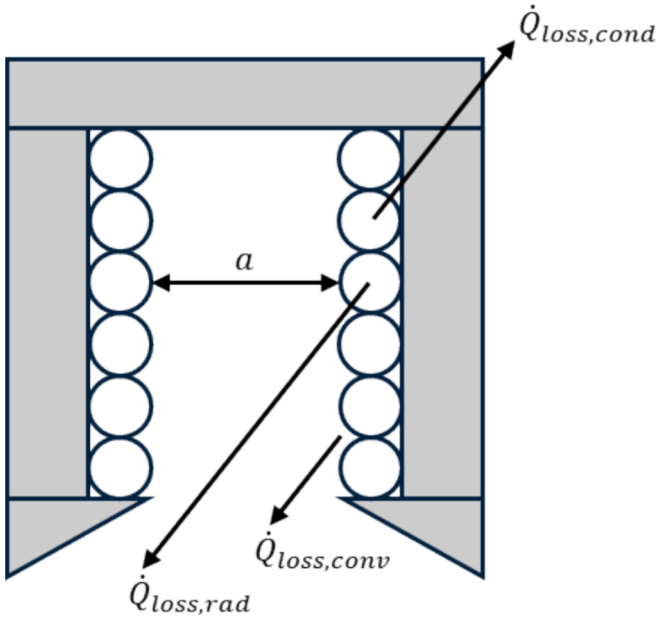

Fig. 7. Solar receiver geometry and dimensions as adapted from Le Roux et al. [8]

into the aperture of the receiver through the use of a low-cost solar dish with an assumed reflectivity of 85 %, an optical error of 10 mrad, a rim angle of 45°, and a dish diameter of 4.8 m for an approximate dish area of 18 m^2. It is assumed that the direct normal irradiance (DNI) is 1000 W/m^2. The solar dish makes use of a two-axis tracking system with an assumed tracking error of 1° and an assumed average receiver angle of 45°. The solar irradiation that enters the aperture is absorbed by the inner walls of the cavity as formed by the stainless-steel coiled tube. This process heats the air flowing through the solar receiver. SolTrace [41], a ray-tracing application, was used to model the rays entering the solar receiver through solar flux mapping techniques [8].

Fig. 7 shows that certain heat loss considerations are made for the solar receiver to represent the realistic environment that the solar receiver is expected to operate in. This includes convective, conductive, and radiative heat losses as defined by Le Roux et al. [8]. The surface temperature of the solar receiver varies under the consideration of different tube sections, as detailed by Le Roux et al. [8], with this surface temperature not being allowed to exceed 1200 K due to the limitations in the solar receiver design conditions [14]. Under the consideration of the various receiver heat losses, the tubes sections, and the surface temperatures, the net heat transfer rate of the solar receiver is determined as per Eq. (9) [8]. To minimise the heat loss, the solar receiver is insulated using ceramic fibre insulation with a thickness of 0.1 m and an emissivity of 0.9 [8]. The model used to characterise the solar receiver processes has been verified against the results of the model by Le Roux et al. [8], as shown in Appendix A. Additionally, the total solar receiver efficiency can be determined as per Eq. (10) [8].

$$\dot{Q}_{net,n} = \dot{Q}_n^* - A_n \sum_{j=1}^{N} F_{n-j}\left(\varepsilon_n \sigma T_{s,n}^4 - \varepsilon_j \sigma T_{s,j}^4\right)$$

$$- A_n F_{n-0}\left(\varepsilon_n \sigma T_{s,n}^4 - \varepsilon_j \sigma T_0^4\right) - \lambda_{recv,n} A_n \left(T_{s,n} - T_0\right)$$

$$- \frac{A_n \left(T_{s,n} - T_0\right)}{\frac{1}{\lambda_o} + \frac{t_{ins}}{k_{ins}}} \tag{9}$$

$$\eta_{SR} = \frac{\dot{Q}_{net}}{\dot{Q}^*} \tag{10}$$

As a general overview of the process to determine the solar heat contribution results in each cycle configuration, only the solar heat and the combustion heat are considered. This means that when the results of the solar heat considered, the heat contribution is determined as per Eq. (11).

$$\%\dot{Q}_{SR} = \frac{\dot{Q}_{SR}}{\dot{Q}_{SR} + \dot{Q}_{CC}} \times 100 \tag{11}$$

2.3. Simple solar cycle analysis

The simple cycles with the inclusion of a solar heat input are solved via an algorithm generated using Python coding. These cycles are modelled under the consideration of many different pressure ratios, with these pressure ratios being divided into three sets of pressure ratios with different intervals between the lowest and highest pressure ratios in the

sets. The first set of pressure ratios is from a compressor pressure ratio of 1.4 to a compressor pressure ratio of 2, in steps of 0.05 to capture more values in the low pressure ratio range. The second set of pressure ratios is from a compressor pressure ratio of 2.125 to a compressor pressure ratio of 2.625, in steps of 0.125 to capture the mid-range pressure ratios intermediately. The third set of pressure ratios includes compressor pressure ratios of 2.75 and 3, in a step size of 0.25 to capture the higher pressure ratios. The generalised solution procedure for solving these cycle configurations is detailed in Fig. 8 for the simple solar LTT cycle, with the remaining simple solar cycles being modelled in a similar manner.

2.4. Recuperated solar cycle analysis

The recuperated solar cycles involve more variable inputs than the simple solar cycles as a direct result of requiring input variables for the recuperator channel height and for the number of recuperator channels. These inputs are incorporated in the Python solution algorithm via the use of Python arrays. The array for the compressor pressure ratio is *[1.4, 1.5, 1.6, 1.8, 2.0, 2.25, 2.5]*, with the recuperator channel height, *b*, in millimetres, being inputted as *[1.50, 2.25, 3.00, 3.75, 4.50]*, and the number of recuperator channels, *n*, being inputted as *[15, 22.5, 30, 37.5, 45]*. This amounts to a total of 175 design points for the recuperated solar layouts. The general Python solution algorithm is structured as per Fig. 9 for the recuperated solar LTT cycle, with the remaining recuperated solar cycles being modelled in a similar manner.

3. Results

The solar cycle configurations were simulated using nine of the best *Garrett Motion* turbocharger combinations, as in the studies by Cockcroft & Le Roux [30,31]. From this, the best main shaft turbocharger, the G25-550 (AR = 0.92), was selected for analysis and for further comparison to each cycle's respective non-solar version. This was done using the best recuperator dimensions to obtain the maximum fuel-based thermal efficiencies while remaining within, or as close as possible to, the maximum allowable gasifier turbine inlet temperature for each cycle that makes use of a recuperator. These recuperator dimensions are indicated in Appendix B. The GBC14-200 and the slightly larger GBC17-250 were identified as the only feasible power turbine options for the various cycle configurations consisting of the G25-550 (AR = 0.92) as the main shaft turbocharger and thus the results of these combinations are discussed. Note that the total thermal efficiencies obtained for each cycle layout are introduced in Appendix C for reference.

For discussion purposes, the utilisation of the first solar receiver placement, prior to the combustion chamber inlet is presented as '(SR-CC)'. Consequently, the second solar receiver placement, prior to the power turbine inlet, is presented as '(SR-PT)'.

3.1. Simple solar cycle results

The results of the simple parallel-flow configuration as well as the simple solar parallel-flow configurations are discussed in the subsections

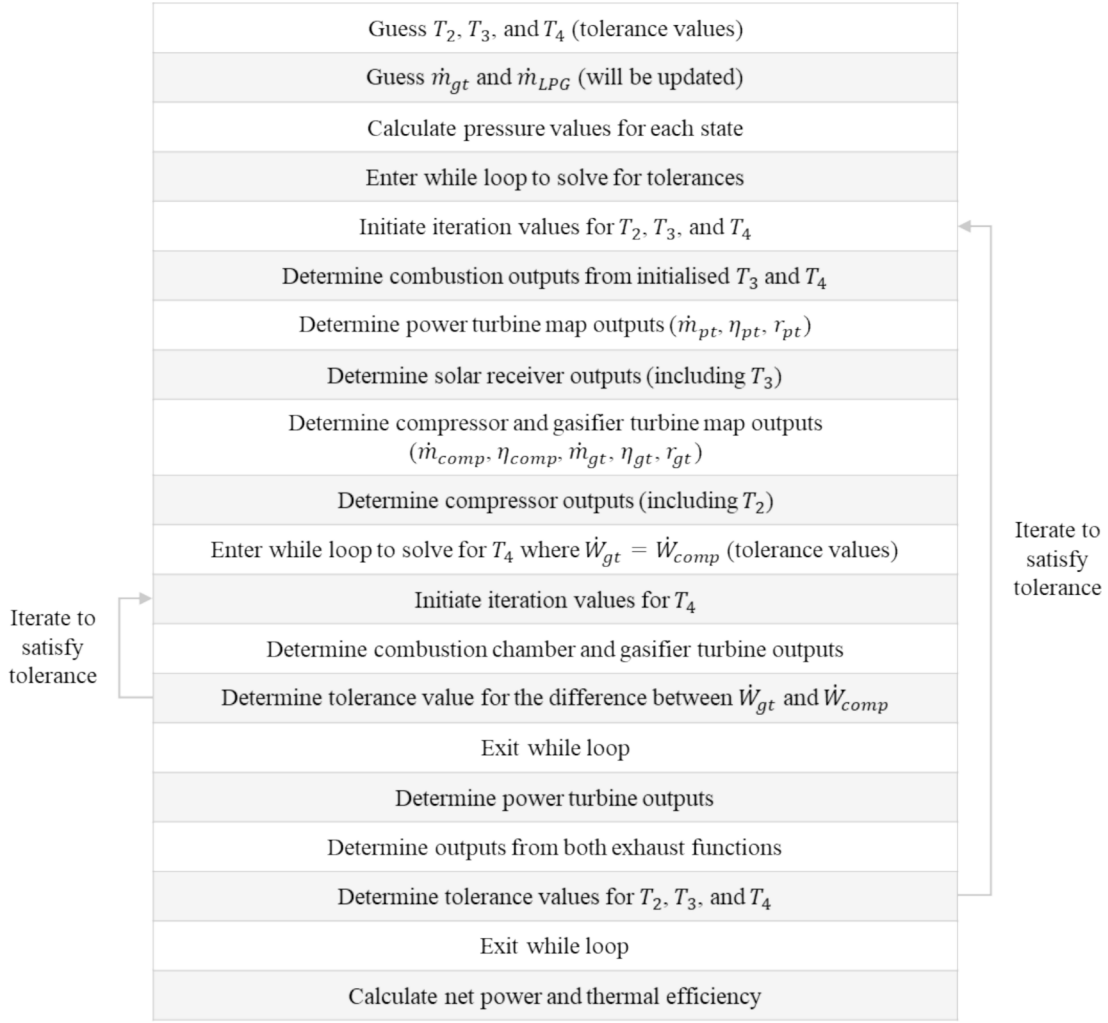

Fig. 8. Solar simple low-temperature turbine (LTT) cycle solution procedure.

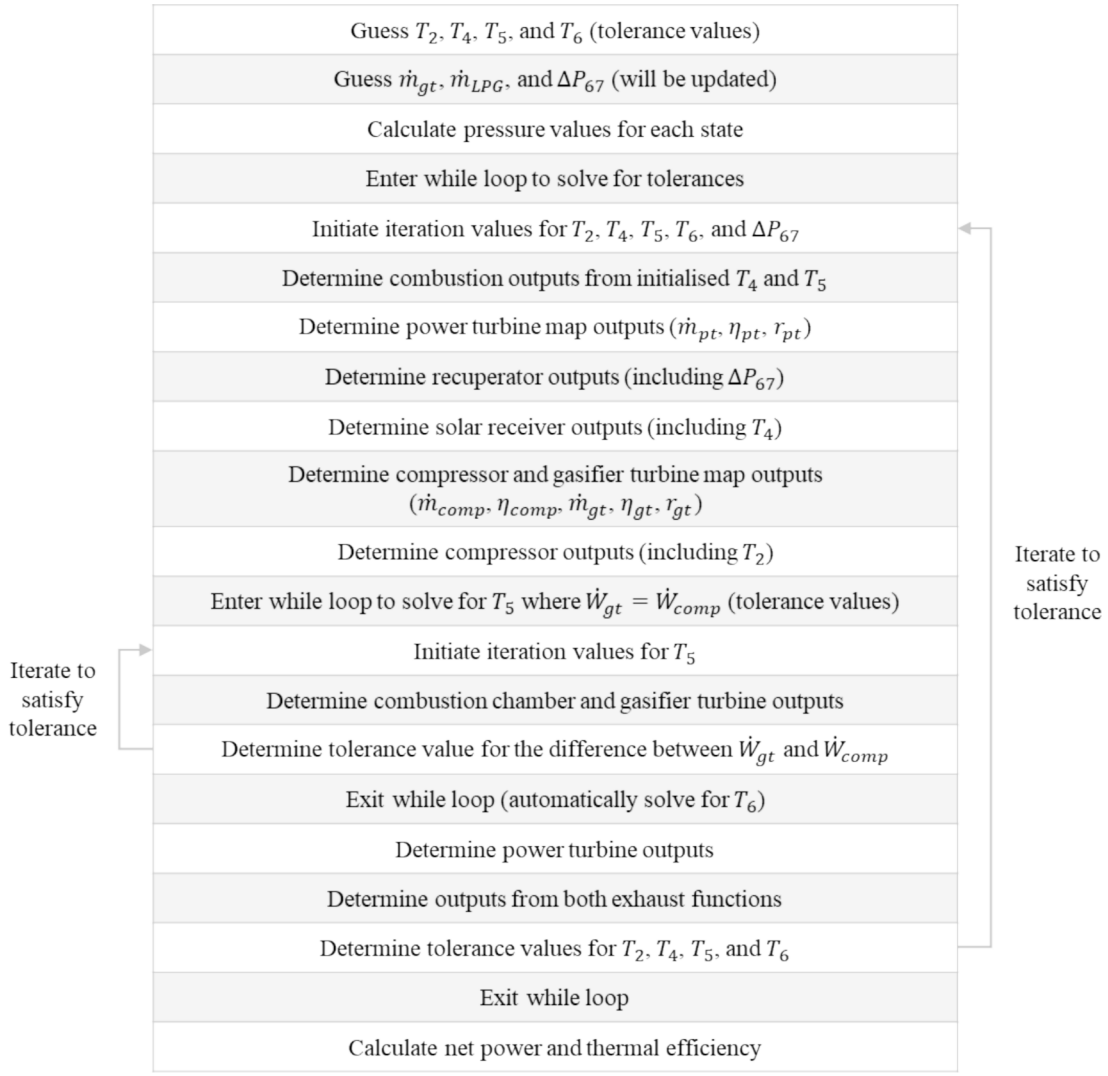

Fig. 9. Recuperated solar low-temperature turbine (LTT) cycle solution procedure.

to follow. This is done with regard to the results for the power outputs and fuel-based thermal efficiencies of the cycles, the temperature constraints, and the contribution of solar heat to the cycles.

3.1.1. *Power and efficiency*

Figs. 10 and 11 show that the power output of the cycle, and the fuel-based thermal efficiency of the cycle, increase with an increase in the compressor pressure ratio, for all the various cycle split-off points and solar receiver placements. Generally, when the larger GBC17-250 is used as the power turbine, the power output of the cycle increases, for all the configurations, under the consideration of the same pressure ratio. Additionally, gasifier turbine inlet temperatures were found to exceed the allowable limit of 1200 K for the simple LTT, the LTT (SR-CC), and the ITT(S) (SR-CC) cycles with the GBC17-250 as the power turbine (as shown in Fig. 12).

Fig. 11 shows that the HTT (SR-CC) cycle offers the best power output and fuel-based thermal efficiency performance at higher pressure ratios. The operation of this HTT (SR-CC) cycle with the GBC17-250 results in the highest simple solar power output and fuel-based thermal efficiency out of all the simple solar cycles, with a power output of 14.5 kW and a fuel-based thermal efficiency of 7.04 %, at a pressure ratio of 2.75. This changes to a maximum fuel-based thermal efficiency of 6.86 % and a power output of 13 kW at a pressure ratio of 3, when the GBC14-200 is used as the power turbine in the mentioned configuration.

For the HTT cycles, the power output of the cycle reduces when a solar heat input is applied to the cycle, with similar, but reduced, values being obtained for the fuel-based thermal efficiency, under the consideration of the same pressure ratio. Thus, a simple solar HTT (SR-CC) cycle does not offer performance improvement over a simple HTT (SR-CC) cycle. This is as a result of the solar receiver reducing the requirement of combustion in the cycle and subsequently reducing the mass flow rate through the gasifier turbine which, as a consequence, reduces the power output. Even though a higher gasifier turbine inlet temperature is applied to the solar HTT cycle (as shown in Fig. 12), this higher inlet temperature is not high enough to offset the lower proportional power turbine mass flow rate (in comparison to the compressor mass flow rate) that is obtained via the operation of the non-solar HTT cycle. However, solutions are obtained for the solar HTT (SR-CC) at high pressure ratios, which have not been obtained for the simple case without solar input. Thus, there is a power output and fuel-based thermal efficiency improvement in the operation of the solar HTT (SR-CC) cycle due to its greater operational range. It is noted that the simple solar HTT (SR-PT) cycle does not obtain any results.

Overall, the simple solar LTT (SR-CC) cycle offers the lowest power output and fuel-based thermal efficiency, when comparing the same compressor pressure ratio. However, the simple solar LTT (SR-PT) cycle obtains the highest cycle fuel-based thermal efficiency, under the consideration of the same pressure ratio. This high fuel-based thermal

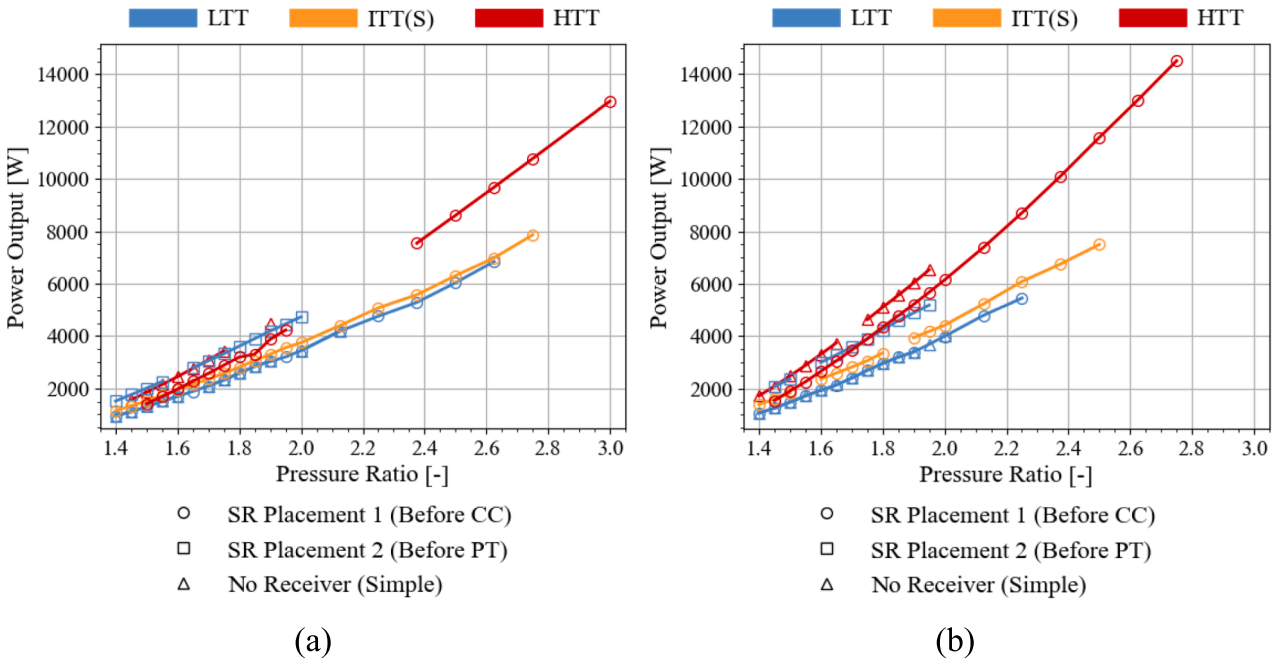

Fig. 10. Power output as a function of compressor pressure ratio for different simple and simple solar cycle configurations – with the G25-550 (AR = 0.92) as the GT with (a) the GBC14-200 as the PT and (b) the GBC17-250 as the PT.

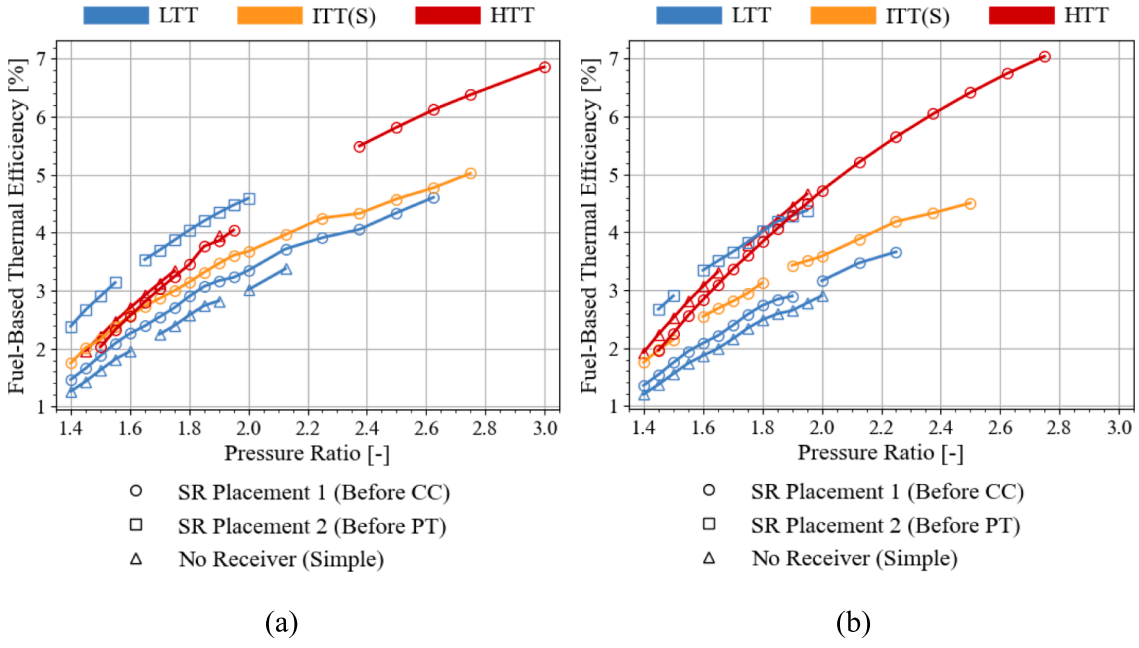

Fig. 11. Fuel-based thermal efficiency as a function of compressor pressure ratio for different simple and simple solar cycle configurations – with the G25-550 (AR = 0.92) as the GT with (a) the GBC14-200 as the PT and (b) the GBC17-250 as the PT.

efficiency is obtained at compressor pressure ratios of between 1.4 and 2.0, as this is the compatible range for the solar LTT (SR-PT) cycle. This cycle obtains fuel-based thermal efficiencies of between 2.3 % and 4.6 % for pressure ratios from 1.4 to 2 when the GBC14-200 is used as the power turbine and fuel-based thermal efficiencies of between 2.7 % and 4.4 % for pressure ratios from 1.45 to 1.95 when the GBC15-250 is used as the power turbine.

For the remaining pressure ratios with the GBC14-200 as the power turbine, the ITT(S) (SR-CC) configuration offers the most feasible performance, especially when considering operation throughout the entire compressor pressure ratio range. The ITT(S) (SR-CC) with the GBC14-200 obtains solutions for every simulated compressor pressure ratio, up to a compressor pressure ratio of 2.75. This shows the effect of pressure loss at low pressure ratio applications, as the ITT(S) (SR-CC) cycle power turbine pressure ratio does not experience as great of a reduction due to pressure loss as in the HTT cycle, which is especially advantageous at lower pressure ratios.

3.1.2. *Temperatures*

With regard to gasifier turbine inlet temperatures, Fig. 12 shows that the second receiver placement (SR-PT) has lower associated gasifier turbine inlet temperatures than the first receiver placement (SR-CC).

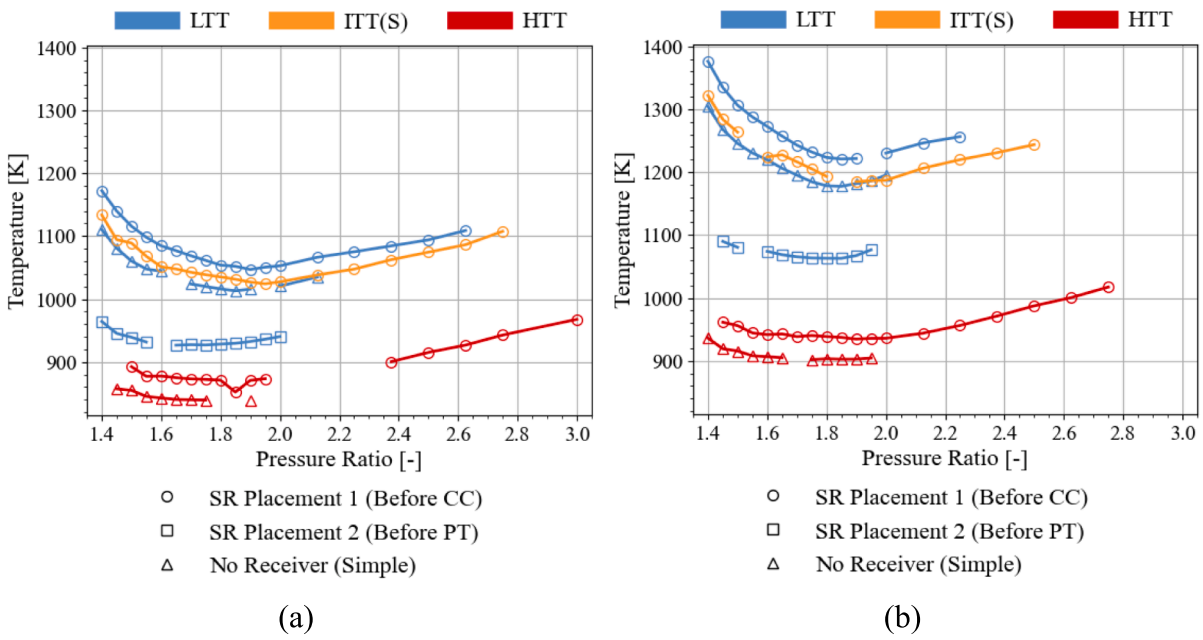

Fig. 12. GT inlet temperature as a function of compressor pressure ratio for different simple and simple solar cycle configurations – with the G25-550 (AR = 0.92) as the GT with (a) the GBC14-200 as the PT and (b) the GBC17-250 as the PT.

This is an important finding because Fig. 12 shows that when the GBC17-250 is used as the power turbine in a simple LTT cycle or in a simple solar LTT (SR-CC) cycle, the gasifier inlet temperatures exceed the limit of 1200 K for a large portion of the operational compressor pressure ratio range, or for the entire pressure ratio range in the instance of the solar LTT (SR-CC) cycle. Thus, receiver placement 2 (SR-PT), allows for lower inlet temperatures with an LTT split-off point in a simple solar cycle.

The second receiver placement (SR-PT) increases the power output of the cycle due to the increased power turbine inlet temperatures, as observed in Fig. 13. The increased power output through the utilisation of the larger GBC17-250 power turbine (as opposed to using the GBC14-200 as the power turbine) increases the feasibility for the implementation of a simple solar LTT cycle. Overall, the HTT cycles have the lowest gasifier turbine inlet temperatures and the LTT cycles have the highest gasifier turbine inlet temperatures. Fig. 14 shows that all the maximum solar receiver surface temperatures are within the limit of 1200 K. Thus, all of the cycles are feasible for operation in terms of remaining within the prescribed temperature limitations.

3.1.3. *Solar contribution and receiver efficiency*

With regard to the utilisation of the solar receiver heat in the cycle, Fig. 15 shows that the proportion of heat supplied to the cycle via the use of the solar receiver decreases as the compressor pressure ratio increases. This is as a result of more heat being required with an increase in the compressor pressure ratio, with a minimal change in the solar

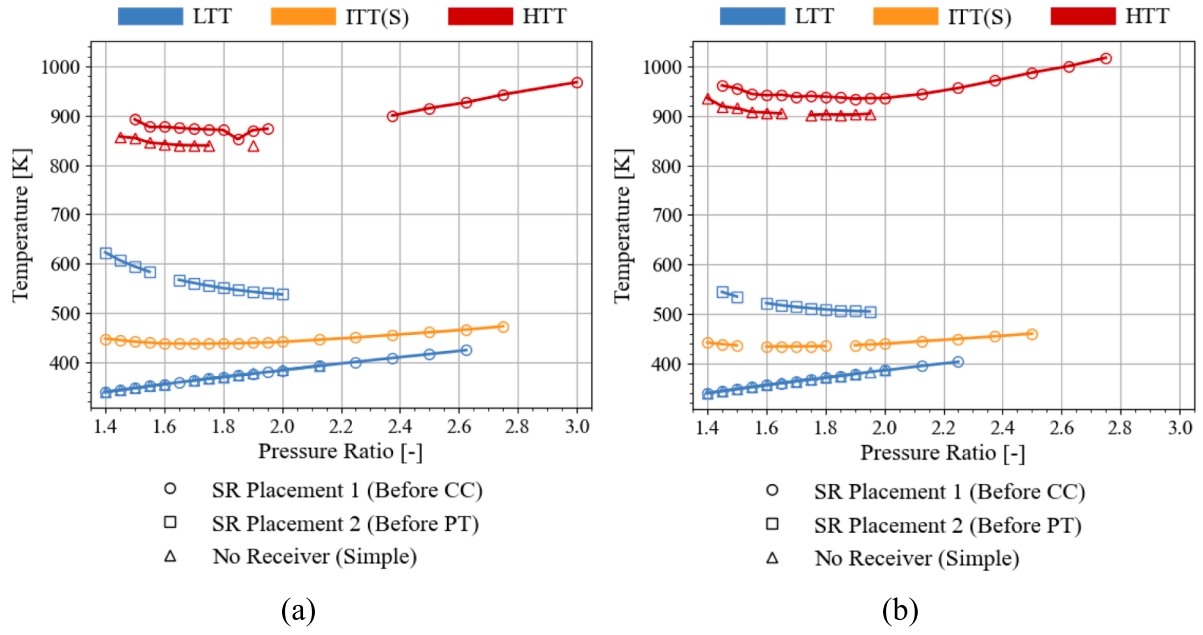

Fig. 13. PT inlet temperature as a function of compressor pressure ratio for different simple and simple solar cycle configurations – with the G25-550 (AR = 0.92) as the GT with (a) the GBC14-200 as the PT and (b) the GBC17-250 as the PT.

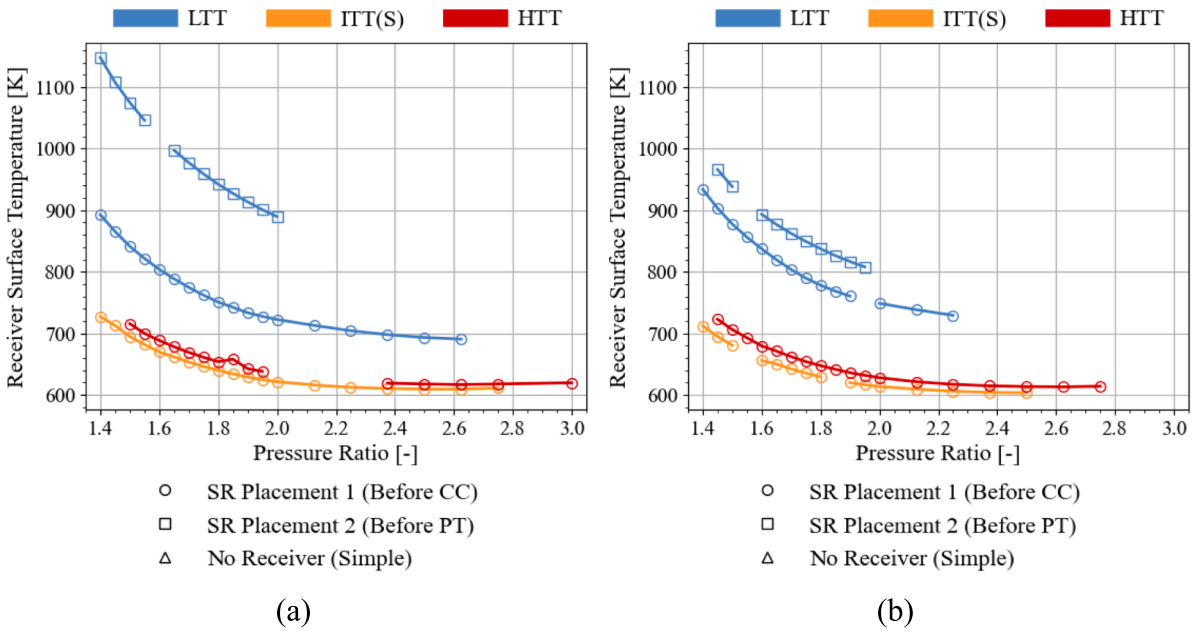

Fig. 14. Maximum solar receiver surface temperature as a function of compressor pressure ratio for different simple and simple solar cycle configurations – with the G25-550 (AR = 0.92) as the GT with (a) the GBC14-200 as the PT and (b) the GBC17-250 as the PT.

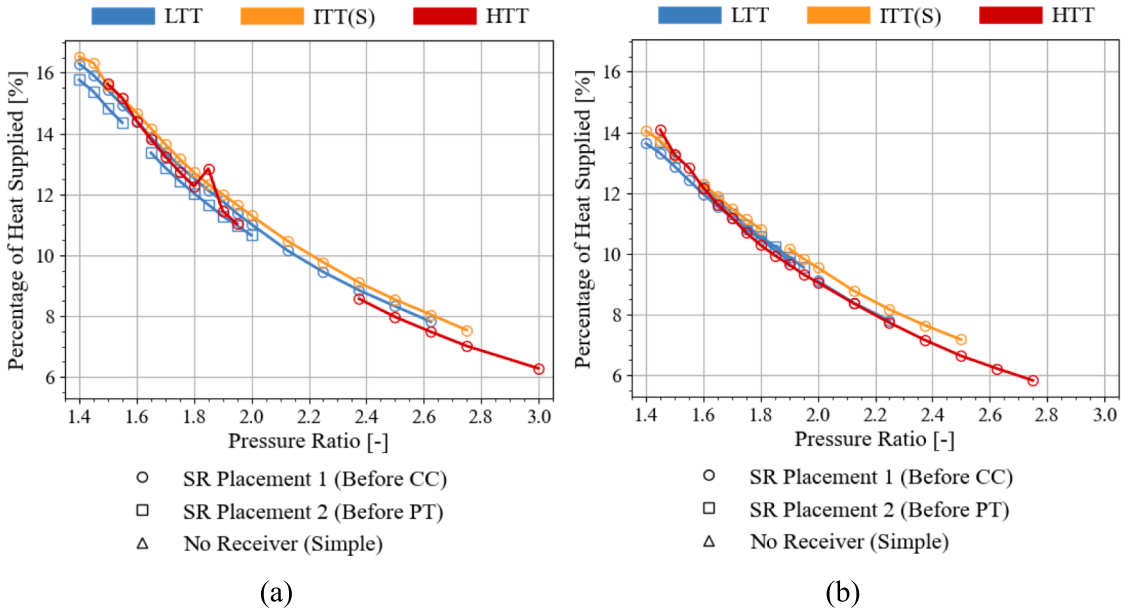

Fig. 15. Proportion of heat supplied by solar receiver as a function of compressor pressure ratio for different simple and simple solar cycle configurations – with the G25-550 (AR = 0.92) as the GT with (a) the GBC14-200 as the PT and (b) the GBC17-250 as the PT.

receiver heat addition over the pressure ratio range. Thus, more fuel combustion is required to supply the required heat to the cycle. Additionally, the ITT(S) (SR-CC) with the GBC14-200 as the power turbine, allows for the greatest solar utilisation for most of the compressor pressure ratio range, with the larger GBC17-250 power turbine having a lower proportional solar utilisation for each configuration. The simple solar LTT (SR-PT) cycle has the lowest proportion of solar heat, with the simple solar LTT (SR-CC) having a slightly higher solar heat proportion but still having the second lowest solar heat proportion at low pressure ratios.

The receiver efficiency, as defined in Eq. (10), of the various configurations and combinations is illustrated in Fig. 16. This figure shows that very high solar receiver efficiencies, in comparison to the study by Le Roux et al. [8], are obtained in the operation of the various parallel-flow simple solar cycle configurations. These high efficiencies are as a result of the low inlet temperatures that are applied to the solar receiver in these simple solar configurations. The low inlet temperatures result in a lower temperature difference between the working fluid in the receiver tubes and the ambient air. This means that heat losses are relatively low for these configurations and thus higher solar receiver efficiencies are obtained.

In the study by Le Roux et al. [8], it is shown that for a recuperated solar cycle, a reduction in the mass flow rate through the solar receiver results in lower receiver efficiencies, and that a reduction in the inlet temperature results in higher receiver efficiencies. When the power turbine inlet has a higher temperature, the power turbine requires a

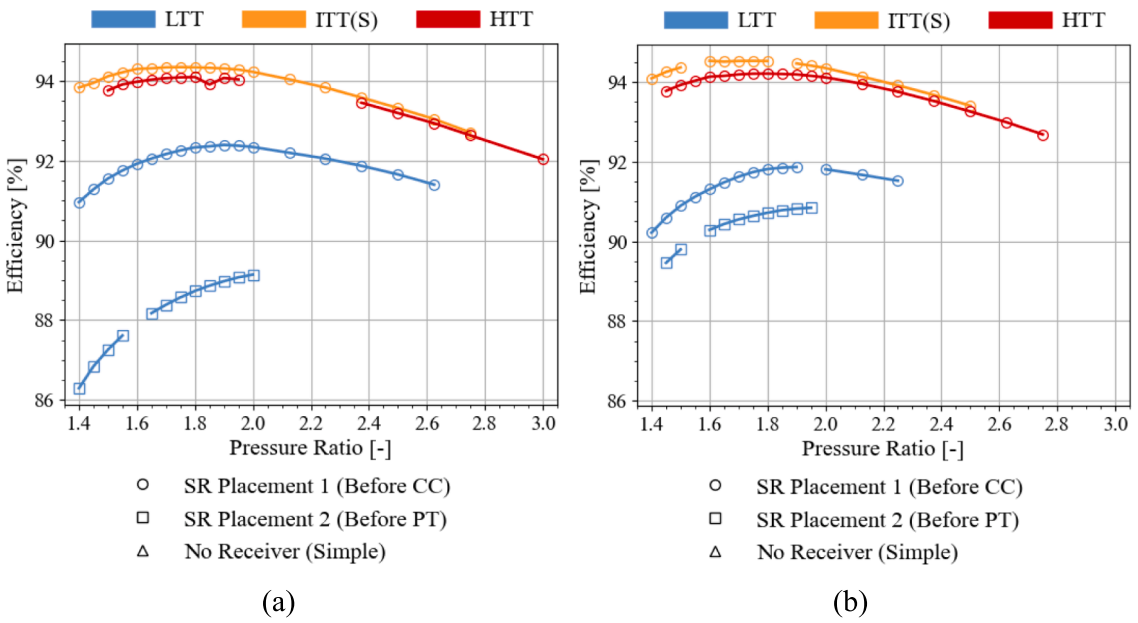

Fig. 16. Solar receiver efficiency as a function of compressor pressure ratio for different simple and simple solar cycle configurations – with the G25-550 (AR = 0.92) as the GT with (a) the GBC14-200 as the PT and (b) the GBC17-250 as the PT.

lower mass flow rate. This is why the ITT(S) (SR-CC) and HTT (SR-CC) configurations have higher receiver efficiencies as these configurations have higher power turbine inlet temperatures, and thus a smaller proportion of the compressor mass flow rate is removed from the compressor flow. This subsequently means that a greater proportional mass flow rate goes through the solar receiver which results in the high receiver efficiencies observed in Fig. 16.

The ITT(S) (SR-CC) configuration has slightly higher receiver efficiencies than the HTT (SR-CC) configuration as a result of having a lower power turbine inlet temperature, even though a greater mass flow rate flows through the power turbine in the ITT(S) (SR-CC) configuration. Similarly, when the GBC17-250 is used as the power turbine, the solar receiver efficiency increases due to the greater mass flow rate required to operate the power turbine, and the subsequent lower mass flow rate that flows through the solar receivers in the ITT(S) (SR-CC) and HTT (SR-CC) configurations.

Moreover, when the LTT configuration is used, the solar receivers for both receiver placements have negligibly different inlet temperatures, due to the compressor outlet temperature (which is the solar receiver inlet temperature for both simple solar receiver placements) being influenced minimally by the solar receiver placement. When the LTT (SR-PT) cycle is used, the power turbine inlet temperature increases, and the power turbine mass flow rate decreases. This power turbine mass flow rate is the same mass flow rate that flows through the solar receiver and is much lower than the mass flow rate that flows through the solar receiver when the first solar receiver placement (SR-CC) is used. This lower mass flow rate results in lower solar receiver efficiencies when the second receiver placement (SR-PT) is used. When the GBC17-250 is used as the power turbine instead of the GBC14-200, for the LTT (SR-PT) cycle, the power turbine mass flow rate increases and thus the solar receiver mass flow rate increases. This is why there is an increase for this configuration and receiver placement when the GBC17-250 is used.

3.2. Recuperated solar cycle results

The recuperated cycle and recuperated solar cycle configurations are to be analysed in this section. The results are generated via a consideration of the best recuperator dimensions for each cycle, as summarised in Appendix B. The gasifier turbine inlet temperature, the power turbine inlet temperature, and the maximum solar receiver surface temperature all need to be within 1200 K, which is shown to be problematic for some of the cycles, as to be discussed in the sub-sections to follow.

3.2.1. Power and efficiency

When considering the power output results of the various parallel-flow configurations, in Fig. 17, the influence of pressure loss on the power output of the cycle starts to become more apparent. This statement is made because for most of the compressor pressure ratio range, the recuperated solar ITT configurations offer greater amounts of power output than the HTT and ITT(S) cycles. The recuperated solar LTT cycles mostly offer the lowest power outputs. Fig. 17 shows that under the consideration of the same pressure ratio, the recuperated solar LTT (SR-CC) achieves the same power output as in the non-solar cycle due to the lack of influence of pressure loss on the power turbine inlet in these cycles. However, for the recuperated solar LTT (SR-PT) cycle, the power output increases due to the heated power turbine inlet. This results in increased fuel-based thermal efficiencies when the LTT (SR-PT) cycle is used.

With regard to fuel-based thermal efficiency, the recuperated solar LTT (SR-PT) extends its applicability as, for most of the pressure ratios, this configuration achieves the highest fuel-based thermal efficiency. This occurs for most of the operational compressor pressure ratio range even though the fuel-based thermal efficiency for this configuration reduces as the compressor pressure ratio increases, as shown in Fig. 18. The recuperated solar LTT (SR-PT) with the GBC17-250 as the power turbine achieves a fuel-based thermal efficiency of between 21.7 % and 15.1 % for pressure ratios between 1.6 and 2.25, with power outputs of between 3 kW and 7.4 kW, respectively. For the same configuration with the GBC14-200 as the power turbine, the cycle achieves a fuel-based thermal efficiency of between 17.8 % and 12.5 % for pressure ratios between 1.5 and 2.5, with power outputs of between 2 kW and 7.7 kW, respectively.

It is noted that at a pressure ratio of 1.5, the non-solar recuperated LTT cycle with the GBC14-200 as the power turbine provides the highest fuel-based thermal efficiency of 19.2 %, fully outperforming all of the recuperated solar cycles for the entire pressure ratio range (with the GBC14-200 power turbine). However, a higher fuel-based thermal efficiency and power output can be obtained when using the recuperated solar LTT (SR-PT) configuration with the GBC17-250 as the power turbine at a pressure ratio of 1.6. It is noted that the recuperated LTT cycle

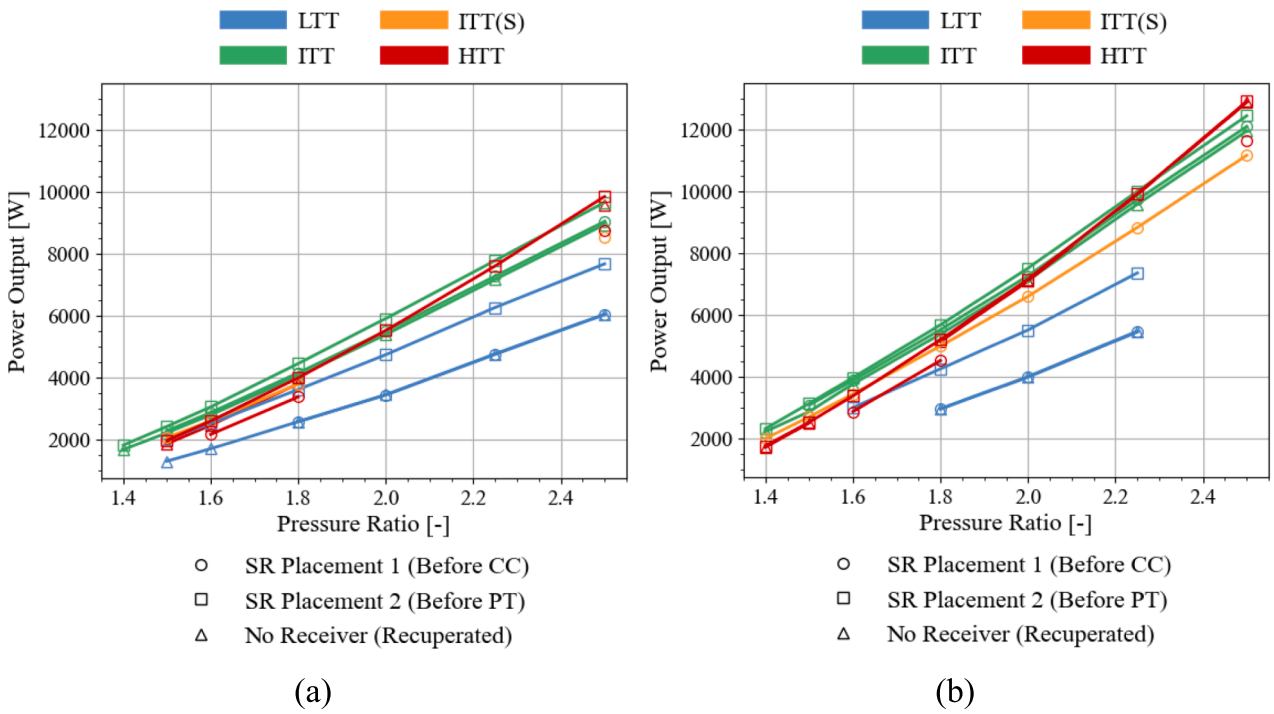

Fig. 17. Power output as a function of compressor pressure ratio for different recuperated and recuperated solar cycle configurations – with the G25-550 (AR = 0.92) as the GT with (a) the GBC14-200 as the PT and (b) the GBC17-250 as the PT.

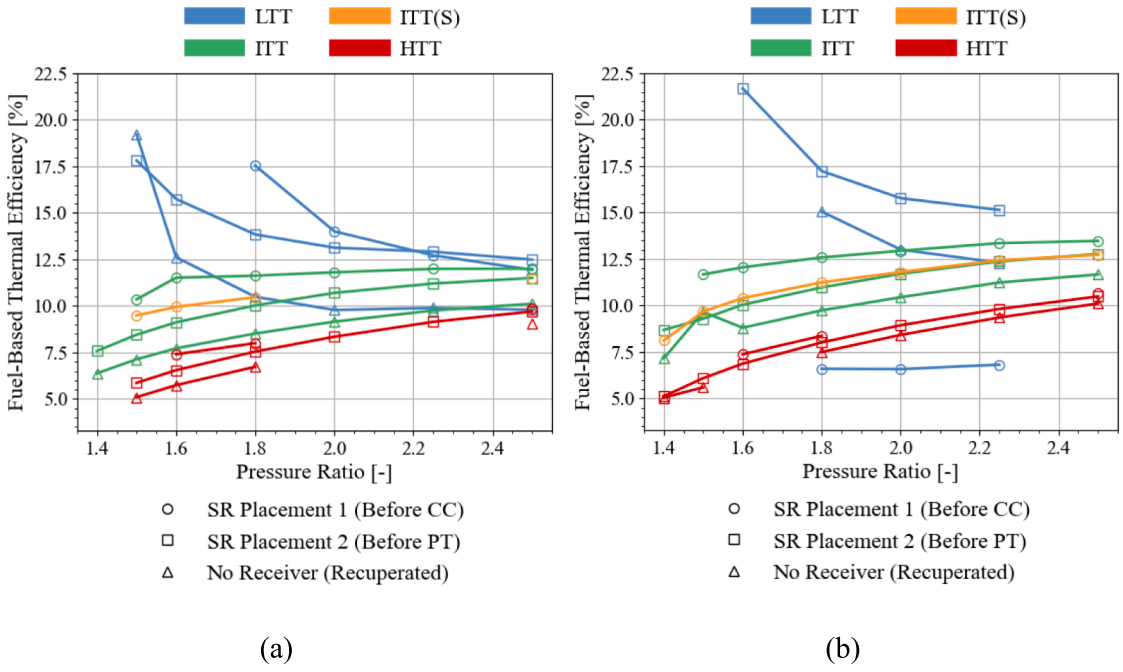

Fig. 18. Fuel-based thermal efficiency as a function of compressor pressure ratio for different recuperated and recuperated solar cycle configurations – with the G25-550 (AR = 0.92) as the GT with (a) the GBC14-200 as the PT and (b) the GBC17-250 as the PT.

and the recuperated solar LTT (SR-CC), both with the GBC17-250 as the power turbine, are not supported for operation due to obtaining high gasifier turbine inlet temperatures (as will be shown in Fig. 19). Additionally, due to high solar receiver surface temperatures, the LTT (SR-CC), the ITT (SR-PT), and the HTT (SR-PT) cycles are not recommended for operation (as will be shown in Fig. 21).

Moreover, the ITT (SR-CC) cycle with the GBC17-250 as the power turbine offers better fuel-based thermal efficiency than the LTT (SR-PT) cycle at pressure ratios greater than 2.25. This ITT (SR-CC) cycle is a good cycle alternative for achieving good fuel-based thermal efficiency results and power output throughout the compressor pressure ratio range, with increasing fuel-based thermal efficiencies of between 10.4 % and 12 % when the GBC14-200 is used as the power turbine, with power outputs of 2.3 kW and 9 kW, respectively, and with increasing fuel-based thermal efficiencies of between 11.7 % and 13.5 % when the GBC17-250 is used as the power turbine, with power outputs of 3 kW and 12 kW,

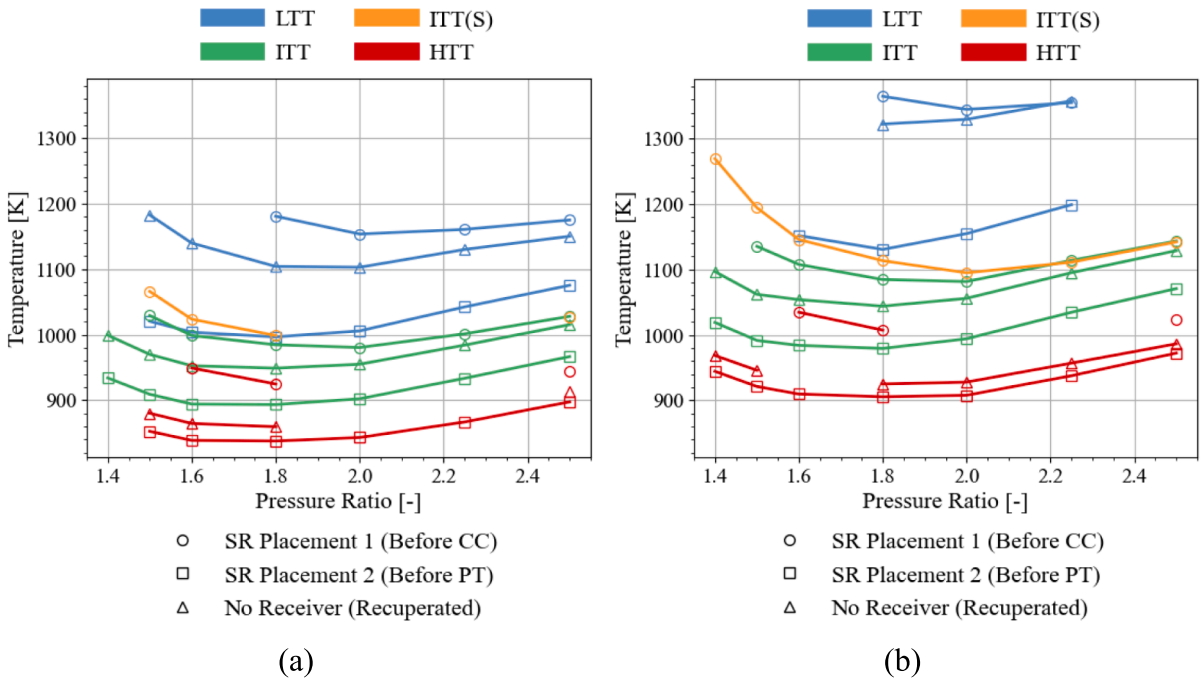

Fig. 19. GT inlet temperature as a function of compressor pressure ratio for different recuperated and recuperated solar cycle configurations – with the G25-550 (AR = 0.92) as the GT with (a) the GBC14-200 as the PT and (b) the GBC17-250 as the PT.

respectively.

Fig. 18 shows that the fuel-based thermal efficiency of the HTT (SR-PT) cycle improves upon the non-solar cycle and the fuel-based thermal efficiency of the HTT (SR-CC) cycle improves more upon the non-solar cycles, but these increases are not as great of an improvement as the recuperator adds to the cycle in the study by Cockcroft & Le Roux [31]. Thus, it is not feasible to implement a recuperated solar HTT (with either receiver placements) due to its minimal performance improvement over the recuperated non-solar HTT cycle.

3.2.2. *Temperatures*

With regard to gasifier turbine inlet temperatures, Fig. 19(a) shows that none of the configurations exceed the maximum allowable gasifier turbine inlet temperature of 1200 K when the GBC14-200 is used as the power turbine. However, via Fig. 19(b), it is shown that, when the GBC17-250 is used as the power turbine, the recuperated LTT and the recuperated solar LTT (SR-CC) cycles do not produce a single solution within the allowable limit of 1200 K. Additionally, the ITT(S) (SR-CC) is not supported for operation at pressure ratios of less than 1.5 due to

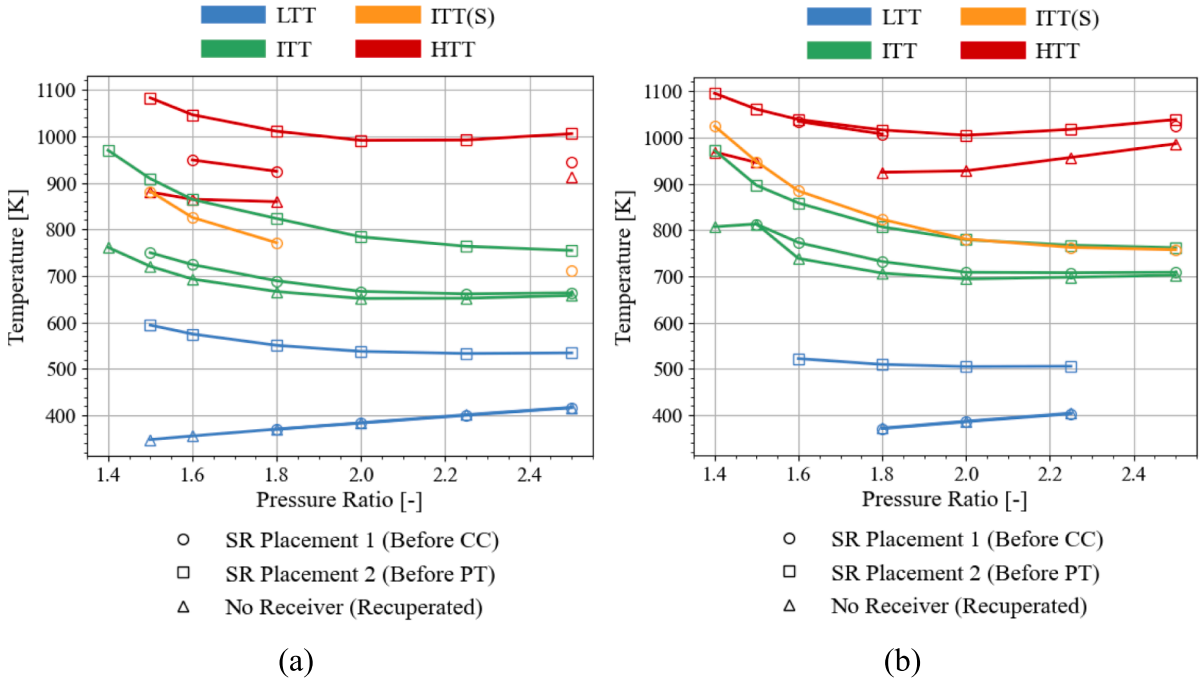

Fig. 20. PT inlet temperature as a function of compressor pressure ratio for different recuperated and recuperated solar cycle configurations – with the G25-550 (AR = 0.92) as the GT with (a) the GBC14-200 as the PT and (b) the GBC17-250 as the PT.

exceeding the limit for the allowable gasifier turbine inlet temperature. All the power turbine inlet temperatures, for the various configurations and combinations, are within the maximum allowable limit of 1200 K, as shown in Fig. 20.

Overall, it is shown via Fig. 19, that the gasifier turbine inlet temperatures increase in comparison to the non-solar cycle for all the split-off points when the first receiver placement is used and decrease in comparison to the non-solar cycle for all the split-off points when the second receiver placement is used. Thus, when a cycle configuration and combination is used with high gasifier turbine inlet temperatures, and the second receiver placement is not used, the use of the second receiver placement may provide feasibility for the combination and split-off point via lowering the gasifier turbine inlet temperatures to be within the allowable limit of 1200 K.

Lastly, the maximum solar receiver surface temperatures are too high (greater than 1200 K) for some pressure ratios in the range, for both power turbine options, when the LTT (SR-CC), ITT (SR-PT), or HTT (SR-PT) configurations are used, as shown in Fig. 21. Thus, when the GBC14-200 is used as the power turbine, the LTT (SR-CC) cycle is not supported for operation at pressure ratios lower than 1.89, the ITT (SR-PT) cycle is not supported for operation at pressure ratios lower than 1.84, and the HTT (SR-PT) cycle is not supported for operation at any pressure ratio. When the GBC17-250 is used as the power turbine, the LTT (SR-CC) cycle is not supported for operation at pressure ratios lower than 1.86, the ITT (SR-PT) cycle is not supported for operation at pressure ratios lower than 1.75, and the HTT (SR-PT) cycle is not supported for operation at pressure ratios lower than 1.9.

3.2.3. *Solar contribution, receiver efficiency, and recuperator effectiveness*

In consideration of the proportion of heat supplied through the solar receiver in the recuperated solar cycles, Fig. 22 shows that in general, the LTT cycles offer the highest proportional solar heat absorption, with the ITT cycles offering the second highest proportional heat absorption when comparing split-off point types. The proportional heat supplied by the solar receiver reduces as the compressor pressure ratio increases, and the second receiver placement has a lower proportional solar receiver heat supply than the first receiver placement, for all the split-off point types except for in the LTT configuration.

The highest proportion of solar heat supply in comparison to combustion occurs when using the recuperated solar LTT (SR-PT) cycle with the GBC14-200 as the power turbine at a compressor pressure ratio of 1.5, with this proportional heat supply being quantified to be 52.1 % of the total solar and combustion heat supplied to the cycle. Fig. 23 shows that the combination of these effects results in the highest solar receiver efficiencies for the LTT (SR-PT) configuration, as this cycle has a lower inlet temperature, in comparison to the other split-off points, and a lower mass flow rate, in comparison to the LTT (SR-CC) cycle. Similarly, the HTT (SR-PT) cycle has the lowest receiver efficiencies as this cycle configuration has an even higher receiver inlet temperature.

Fig. 24 shows that the recuperator effectiveness values all decrease as the pressure ratio increases. The LTT cycles offer the highest effectiveness values and the HTT cycles offer the lowest effectiveness values, as in the study by Cockcroft & Le Roux [31]. This is not observed for the LTT (SR-CC) cycle with the GBC17-250 as the power turbine, as this cycle has recuperator geometry that does not result in the highest fuel-based thermal efficiency but rather in the lowest gasifier turbine inlet temperatures as detailed in Appendix B. Fig. 24 shows that the recuperator effectiveness increases, with reference to the non-solar configurations, for each split-off point that utilises the first receiver placement. When the second receiver placement is used, the recuperator effectiveness decreases to slightly less than in the non-solar cycle.

4. Conclusion

In conclusion, different simple solar cycle and recuperated solar cycle configurations have been investigated in a steady-state analysis for specific conditions in Pretoria, South Africa, using different commercial turbocharger combinations. An analysis of the influence that the placement of the solar receiver has on the cycle was performed. The best main shaft turbocharger, the G25-550 (AR = 0.92), has been investigated, with regard to cycle performance, for both the GBC14-200 and the GBC17-250 power turbine options. Note that the results of the study are for a steady-state analysis, assumed at peak conditions of 1000 W/m^2 solar direct normal irradiance, and would change in an off-design analysis or for yearly simulations with ambient fluctuations.

Conclusions are to be made for a simple solar parallel-flow cycle, considering the simulated cycle conditions. For low pressure ratio applications, consisting of compressor pressure ratios between 1.4 and 2, a

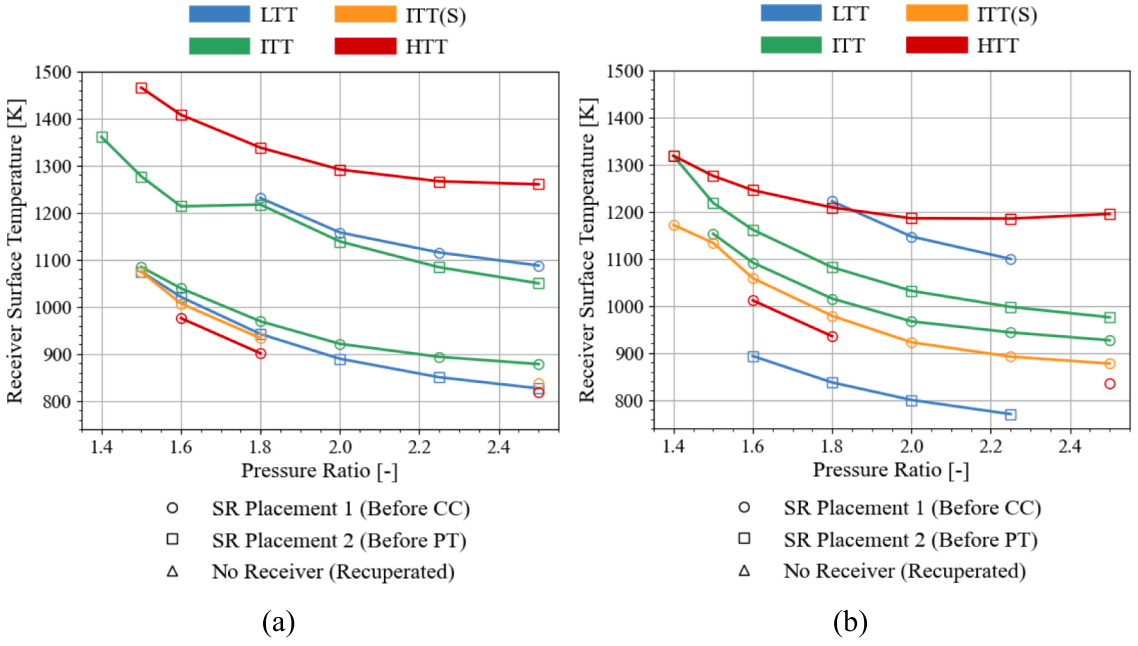

Fig. 21. Maximum solar receiver surface temperature as a function of compressor pressure ratio for different recuperated and recuperated solar cycle configurations – with the G25-550 (AR = 0.92) as the GT with (a) the GBC14-200 as the PT and (b) the GBC17-250 as the PT.

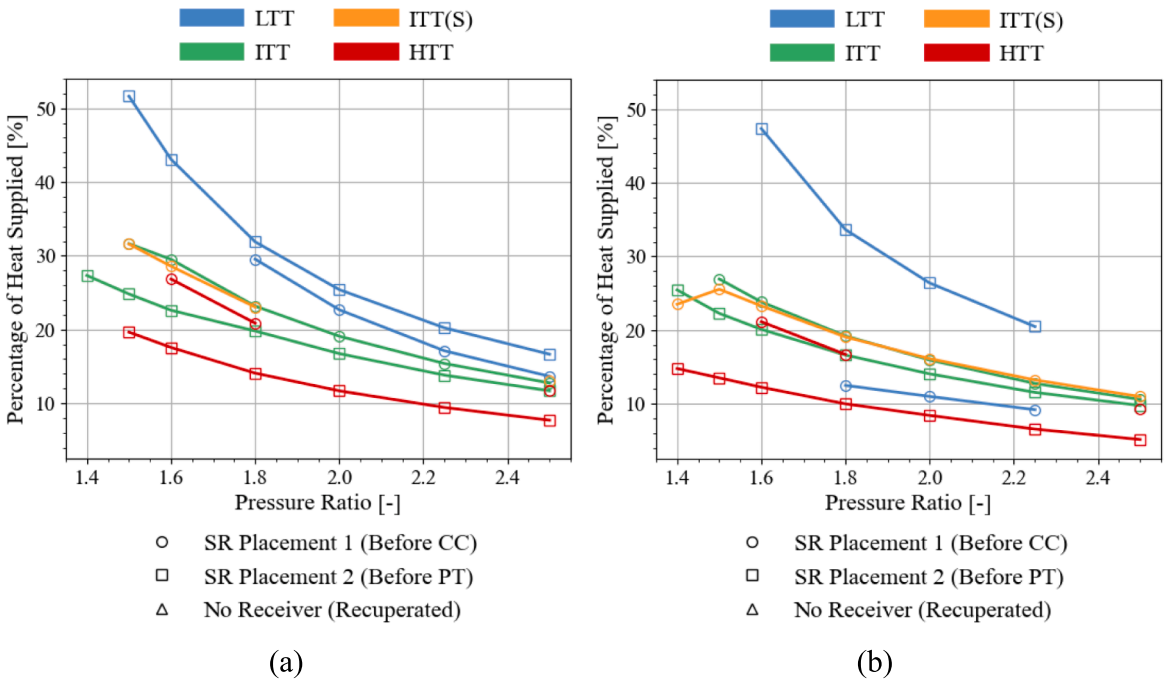

Fig. 22. Proportion of heat supplied by solar receiver as a function of compressor pressure ratio for different recuperated and recuperated solar cycle configurations – with the G25-550 (AR = 0.92) as the GT with (a) the GBC14-200 as the PT and (b) the GBC17-250 as the PT.

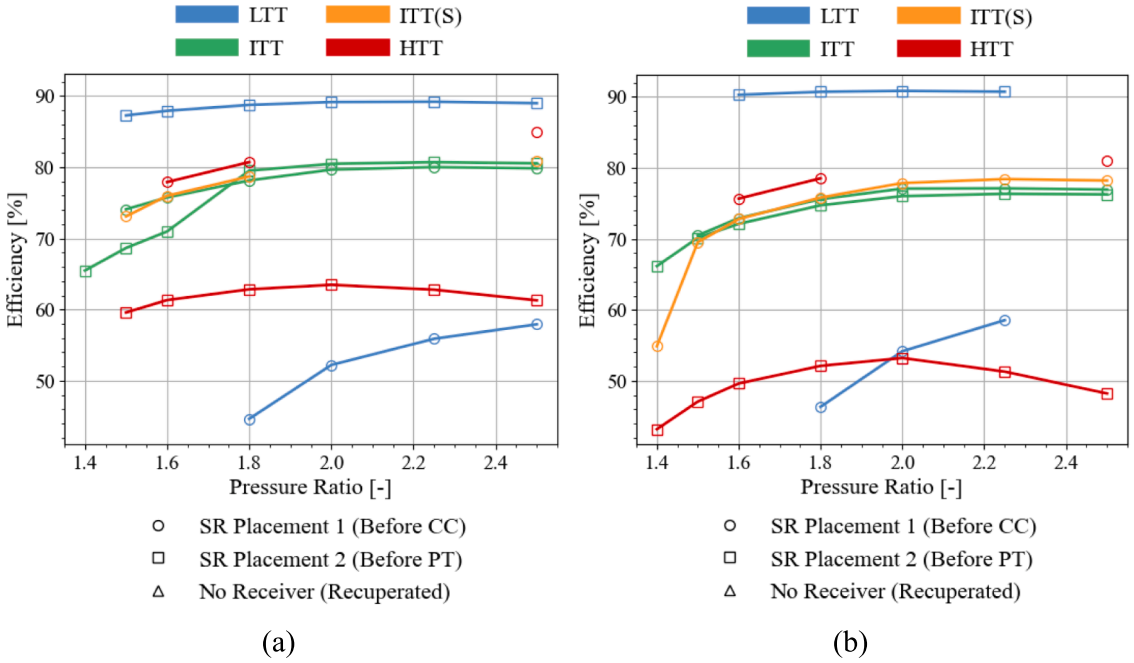

Fig. 23. Solar receiver efficiency as a function of compressor pressure ratio for different recuperated and recuperated solar cycle configurations – with the G25-550 (AR = 0.92) as the GT with (a) the GBC14-200 as the PT and (b) the GBC17-250 as the PT.

simple solar low-temperature turbine (LTT) configuration, with the receiver placed prior to the power turbine inlet, offers the best power output and fuel-based thermal efficiency results. For high pressure ratio applications, consisting of compressor pressure ratios between 2.375 and 3, a high-temperature turbine (HTT) configuration, with the receiver placed before the combustion chamber inlet, offers the best power output and fuel-based thermal efficiency results. This HTT cycle is capable of offering up to 13 kW of power output at a thermal efficiency of 6.86 % when the GBC14-200 is used as the power turbine. The GBC17-250 power turbine in this HTT configuration outperforms all the solar parallel-flow cycles at compressor pressure ratios of greater than 1.9, with a power output of 14.5 kW and a fuel-based thermal efficiency of 7.04 %, at a pressure ratio of 2.75. This cycle obtains the highest fuel-based thermal efficiency when a recuperator is not incorporated into the cycle setup. The operation of a cycle without a recuperator is beneficial when it comes to reducing the capital costs of the cycle due to excluding the cost associated with manufacturing a recuperator.

Conclusions are to be made for a recuperated solar cycle, considering

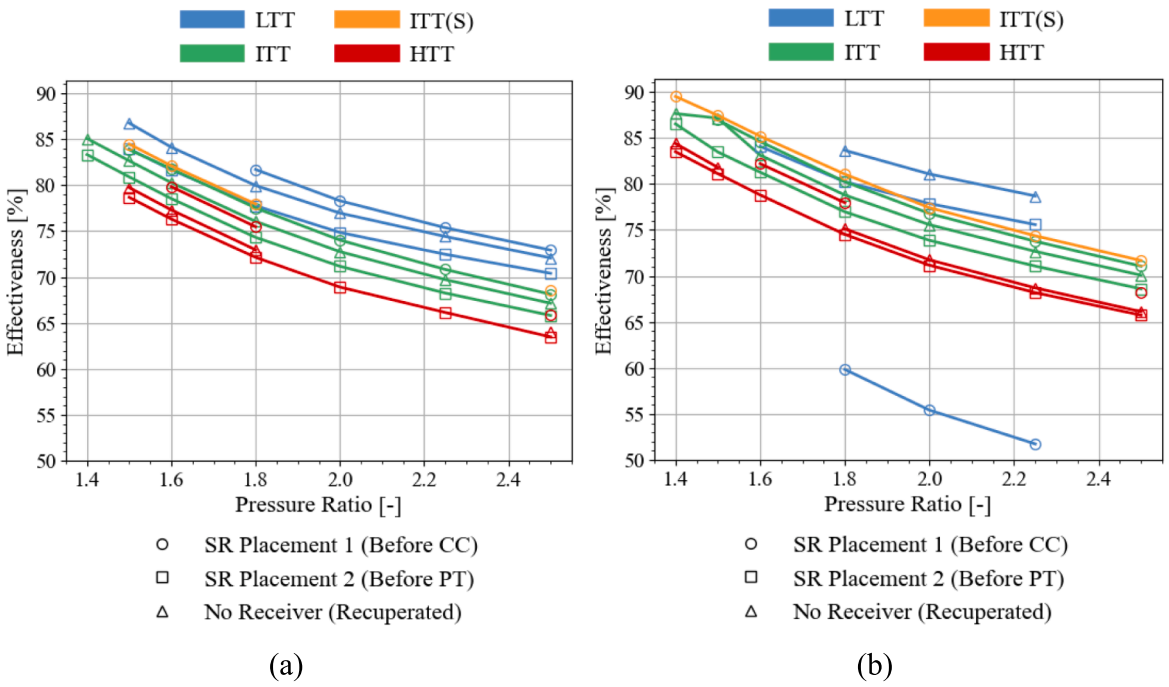

Fig. 24. Recuperator effectiveness as a function of compressor pressure ratio for different recuperated and recuperated solar cycle configurations – with the G25-550 (AR = 0.92) as the GT with (a) the GBC14-200 as the PT and (b) the GBC17-250 as the PT.

the simulated design conditions. When considering the GBC17-250 as the power turbine, the recuperated solar LTT cycle, with the solar receiver placed directly before the power turbine inlet, offers the best fuel-based thermal efficiency of 21.7 %, with a power output of 3 kW, at a pressure ratio of 1.6. This is achieved while maintaining gasifier turbine inlet temperatures within the allowable turbine inlet temperature. However, the greatest power outputs, of up to 12 kW, are obtained at high pressure ratios. For this, the recuperated solar ITT cycle, with the solar receiver placed prior to the combustion chamber inlet, offers the best cycle fuel-based thermal efficiency of 13.5 % at the highest simulated compressor pressure ratio of 2.5, for the same power turbine option.

Overall, the recuperated solar LTT with the solar receiver placed prior to the power turbine inlet obtains the highest fuel-based thermal efficiency results, for the simulated steady-state conditions. The recuperated solar LTT cycle offers the best performance at a low pressure ratio of 1.6 to obtain the maximum fuel-based thermal efficiency. This maximum fuel-based thermal efficiency reduces the running costs associated with the operation of the cycle as less LPG needs to be consumed per kilowatt to operate the cycle. Additionally, operating at low pressure ratios allows for an extension of the lifespan of the cycle turbomachinery in comparison to higher pressure ratio applications. This is particularly important because a viable CSP cycle is expected to operate continuously when solar energy is available in the daytime (unlike a car engine where automotive turbochargers are usually used) and continuous operation at high pressure ratios can be detrimental to the lifespan of the cycle's turbochargers. During periods of operation when there is little to no availability of solar energy, the cycle operation can be suspended or more fuel can be burnt in the combustion process to supplement the required cycle heat. This would reduce the thermal efficiency of the cycle but would still allow for cycle operation, however, the operating point might be affected. This would need to be investigated in future work to ascertain the dynamic effects on cycle performance when there is no available solar energy or when the DNI is a function of time and not the modelled 1000 W/m^2 constant DNI value of the current study.

Furthermore, there are further cycle improvements that can be investigated in later studies. One possible improvement may arise from adding a thermal energy storage unit to the recommended cycle for operation during times where the DNI that the cycle is exposed to is low. This would reduce the requirement for combustion during these periods. Additionally, the energy utilisation of the power cycle can be considered with regard to its ability to provide heat for cogeneration applications, such as water heating. Furthermore, an investigation can be done regarding turbine inlet air cooling (TIAC) to reduce the high inlet temperatures of the simple solar and recuperated solar cycles where high inlet temperatures reduce the feasibility of the configurations. The option of two different solar receivers in a parallel-flow cycle, introduces the possibility of utilising a multi-dish configuration wherein the advantages of both receiver placements can be utilised for better cycle performance. Other solar dish sizes and a receiver with a variable tube diameter can be investigated for further optimisation using entropy generation minimisation. An off-design analysis should also be incorporated to determine how the cycles would respond in instances where the cycle is exposed to different ambient and solar conditions and to yearly temporal and solar fluctuations. Lastly, an economic analysis can be done regarding the cycles in the study to determine the cost savings associated with operating a cycle with a higher fuel-based thermal efficiency.

CRediT authorship contribution statement

C.C. Cockcroft: Writing – review & editing, Writing – original draft, Visualization, Validation, Software, Methodology, Investigation, Formal analysis, Data curation, Conceptualization. **W.G. Le Roux:** Writing – review & editing, Supervision, Methodology, Funding acquisition, Conceptualization.

Declaration of competing interest

The authors declare that they have no known competing financial interests or personal relationships that could have appeared to influence the work reported in this paper.

Acknowledgements

The authors would like to extend their sincere gratitude to the Department of Science and Innovation (DSI) for their funding in support of the research conducted by the UP Solar Thermal Spoke as part of the Renewable Energy Hub and Spokes Programme.

Appendix A. Solar receiver model verification

To verify the Python model, the results of the Python model are compared to the results by Le Roux et al. [8], under the consideration of a receiver inlet temperature of 1000 K, an inlet pressure of 86.6 kPa, and an air mass flow rate of 0.08 kg/s, with the three extra coils that have been removed in the current study being added for verification purposes. To directly compare the two different models, profiles for the receiver surface temperatures, net heat transfer rates, and air temperatures over the tubes, were plotted as per Fig. A1. Overall, the two models output similar results, with slight deviations through the profiles. These deviations are considered to be as a result of updated properties using the CoolProp [32] thermodynamic property library in the Python model.

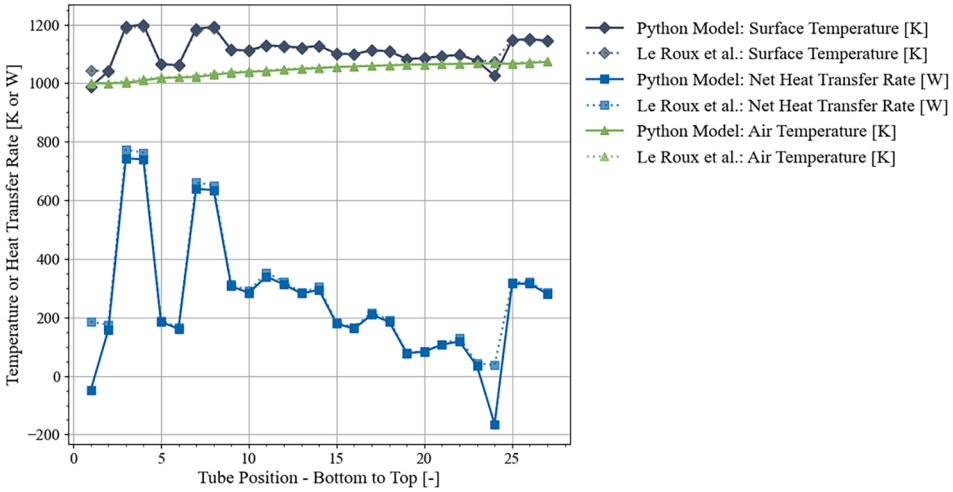

Fig. A1. Verification for solar receiver model temperatures and net heat transfer rate

The Python model uses an iterative process to account for the outlet pressure of the receiver to update the outlet fluid thermodynamic properties using CoolProp, which is not done in the reference study. This iterative process in the Python model is used to update all the enthalpy values in the model, instead of using a constant specific heat as in the study by Le Roux et al. [8]. All of these factors influence the output of the Python model; however, the Python results are still similar to the reference results and thus the Python model accurately characterises the solar receiver.

Appendix B. . Best recuperator dimensions for each recuperated configuration

The best-case recuperator dimensions for each recuperated and recuperated solar configuration, over the entire simulated pressure ratio range, is summarised in Table B1. In brackets next to the configuration type, in Table B1, the number indicates the receiver placement of the configuration, with (SR-CC) indicating that the receiver is at the combustion chamber inlet, and (SR-PT) indicating that the receiver is at the power turbine inlet.

Table B1
Recuperator dimensions used for each recuperated and recuperated solar configuration for different PT options with the G25-550 (AR = 0.92) as the GT.

Power Turbine	Cycle Type	Cycle Configuration	Number of Channels [-]	Channel Height [mm]
GBC14-200	Recuperated	LTT	45.0	1.50
		ITT	45.0	1.50
		HTT	45.0	3.00
	Recuperated Solar	LTT (SR-CC)	45.0	3.00
		LTT (SR-PT)	45.0	1.50
		ITT (SR-CC)	45.0	2.25
		ITT (SR-PT)	45.0	2.25
		ITT(S) (SR-CC)	45.0	2.25
		HTT (SR-CC)	45.0	3.00
		HTT (SR-PT)	45.0	3.75
GBC17-250	Recuperated	LTT	45.0	1.50
		ITT	45.0	1.50
		HTT	45.0	3.00
	Recuperated Solar	LTT (SR-CC)	15.0	4.50
		LTT (SR-PT)	45.0	3.00
		ITT (SR-CC)	45.0	2.25
		ITT (SR-PT)	45.0	3.00
		ITT(S) (SR-CC)	45.0	2.25
		HTT (SR-CC)	45.0	3.00
		HTT (SR-PT)	45.0	3.00

The best-case recuperator dimensions are selected based on the best-case results for obtaining the maximum cycle fuel-based thermal efficiency, with a consideration of the compatible pressure ratio range, for each configuration and compressor pressure ratio, while remaining within the gasifier turbine inlet temperature limit of 1200 K. This is the reason why the results of the recuperated solar LTT (SR-CC) configuration with the GBC17-250 as the power turbine is the only result that requires 15 channels and a channel height of 4.5 mm – these recuperator geometry conditions result in the lowest gasifier turbine inlet temperatures.

Appendix C. . Total thermal efficiency results of the solar cycles

The total thermal efficiency results of the various simple solar configurations are shown in Fig. C1, calculated using Eq. (2). From this figure, it is shown that the HTT (SR-CC) configuration with the GBC17-250 as the power turbine allows for the overall highest total thermal efficiency of 6.6 % (at a pressure ratio of 2.75) and for the highest total thermal efficiencies at high pressure ratios. The simple solar LTT (SR-CC) cycles allow for the lowest total thermal efficiencies with values that improve negligibly over the non-solar simple LTT cycle. At low pressure ratios the LTT (SR-PT) cycles allow for the highest total thermal efficiencies. These results are very similar to the analysis pertaining to the fuel-based thermal efficiencies, except that the solar cycles do not offer as good of a performance improvement over the non-solar cycles, in terms of total thermal efficiency.

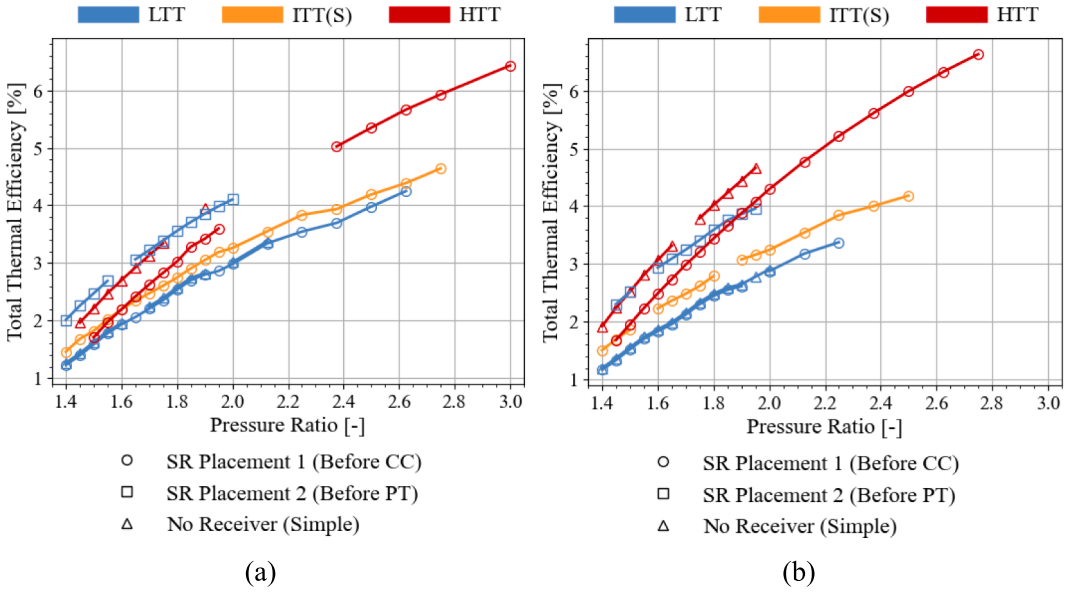

Fig. C1. Total thermal efficiency as a function of compressor pressure ratio for different simple and simple solar cycle configurations – with the G25-550 (AR = 0.92) as the GT with (a) the GBC14-200 as the PT and (b) the GBC17-250 as the PT

For the recuperated solar cycles, the total thermal efficiency results are shown in Fig. C2, as calculated from Eq. (2). It is shown that the best overall total thermal efficiency of 19.2 %, within all the temperature limits, is obtained for the non-solar LTT cycle at a pressure ratio of 1.5. Therefore, the solar cycles are not able to obtain overall better total thermal efficiency results than the non-solar cycle.

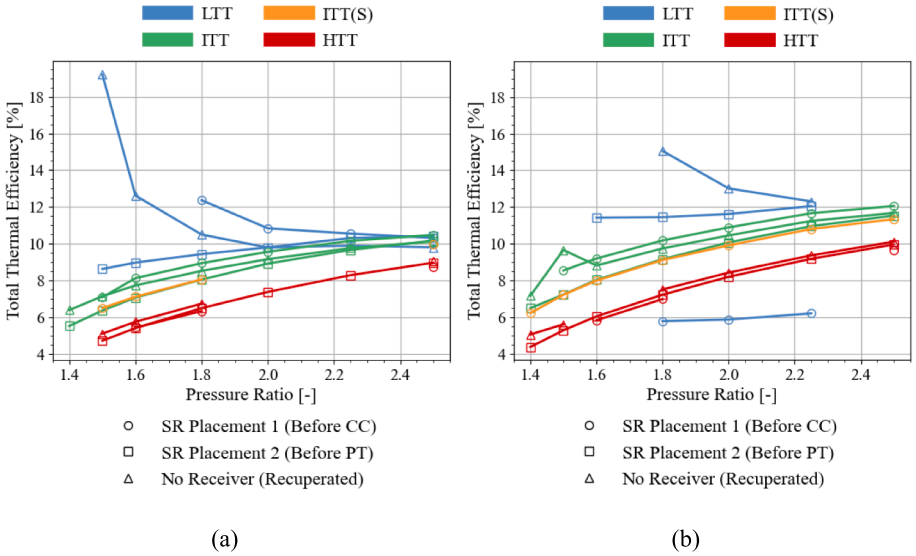

Fig. C2. Total thermal efficiency as a function of compressor pressure ratio for different recuperated and recuperated solar cycle configurations – with the G25-550 (AR = 0.92) as the GT with (a) the GBC14-200 as the PT and (b) the GBC17-250 as the PT

For the solar cycles that utilise the 'SR-CC' placement, the ITT total thermal efficiency improvement only improves slightly upon the non-solar

cycle. The LTT (SR-CC) cycle with the GBC14-200 as the power turbine improves slightly more over the non-solar cycle on a per-pressure-ratio basis. This LTT (SR-CC) cycle improvement over the non-solar cycle decreases as the pressure ratio increases and is only applicable for pressure ratios between 1.8 and 2.42. The LTT (SR-CC) cycle obtains a maximum total thermal efficiency of 12.4 %, at a pressure ratio of 1.8, which is 35.4 % lower than the maximum total thermal efficiency obtained via the non-solar recuperated LTT cycle. The placement of the solar receiver prior to the combustion chamber inlet also has higher gasifier turbine inlet temperatures that limit the selection of the best geometry and further limits the operational pressure ratio ranges of the cycles.

The 'SR-PT' placement mostly does not offer better total thermal efficiency than the non-solar counterparts of each split-off point. This shows the value of evaluating the cycles using fuel-based thermal efficiency rather than total thermal efficiency as total thermal efficiency does not indicate a lower usage of fuel in the cycles. The total thermal efficiency rather indicates how the cycle utilises the heat entering the cycle to produce the cycle power output.

References

[1] J.K. Swanepoel, W.G. Le Roux, A.S. Lexmond, J.P. Meyer, Helically coiled solar cavity receiver for micro-scale direct steam generation, Appl. Therm. Eng. 185 (2021).

[2] International Trade Administration, South Africa - Energy, International Trade Administration | Trade.gov, 26 January 2024. [Online]. Available: https://www.trade.gov/country-commercial-guides/south-africa-energy. [Accessed 16 August 2024].

[3] K.E. Elfeky, M. Hosny, A.G. Mohammed, W. Chu, S.A. Khatwa, Q. Wang, Performance optimization of the parabolic trough power plant using a dual-stage ensemble algorithm, Appl. Therm. Eng. 249 (2024).

[4] Department of Mineral Resources & Energy, South Africa, "Energy Resources," 2024. [Online]. Available: https://www.dmre.gov.za/energy-resources/energy-sources/renewable-alternative-fuels/solar-power. [Accessed 15 August 2024].

[5] S. Potts, D.R. Walwyn, An exploratory study of the South African concentrated solar power sector using the technological innovation systems framework, J. Energy Southern Africa 31 (2) (2020) 1–18.

[6] A.E. Gürel, Ü. Ağbulut, H. Bakır, A. Ergün, G. Yıldız, A state of art review on estimation of solar radiation with various models, Heliyon 9 (2) (2023), 1–26.

[7] W.G. Le Roux, T. Bello-Ochende, J.P. Meyer, Optimisation of an open rectangular cavity receiver and recuperator used in a small-scale solar thermal Brayton cycle with thermal losses, 10th, International Conference on Heat Transfer, Fluid Mechanics and Thermodynamics (HEFAT2014, Orlando, Florida, USA), (July, 2014).

[8] W.G. Le Roux, T. Bello-Ochende, J.P. Meyer, The efficiency of an open-cavity tubular solar receiver for a small-scale solar thermal Brayton cycle, Energ. Conver. Manage. 84 (2014) 457–470.

[9] W. G. Le Roux, J. P. Meyer, Modeling the Small-Scale Dish-Mounted Solar Thermal Brayton Cycle," in SOLARPACES 2015: International Conference on Concentrating Solar Power and Chemical Energy Systems, Cape Town, South Africa, 2015, AIP Conf. Proc. 1734, 060002 (2016), https://doi.org/10.1063/1.4949144.

[10] W.G. Le Roux, Feasibility study of a hybrid small-scale dish-mounted solar thermal brayton cycle with cogeneration, in: Proceedings of the 16th International Heat Transfer Conference (IHTC-16), Beijing, 2018 (DOI: 10.1615/IHTC16.nee.024185).

[11] W.G. Le Roux, A. Sciacovelli, Recuperated solar-dish Brayton cycle using turbocharger and short-term thermal storage, Sol. Energy 194 (2019) (2019) 569–580.

[12] C. Roosendaal, J.K. Swanepoel, W.G. Le Roux, Performance analysis of a novel solar concentrator using lunar flux mapping techniques, Sol. Energy 206 (2020) 200–215.

[13] G. Humbert, C. Roosendaal, J.K. Swanepoel, H.M. Navarro, W. Le Roux, A. Sciacovelli, Development of a latent heat thermal energy storage unit for the exhaust of a recuperated solar-dish Brayton cycle, Appl. Therm. Eng. 216 (2022) 1–15.

[14] J.K. Swanepoel, W.G. Le Roux, C. Roosendaal, S.H. Madani, G. De Wet, T. Nikolaidis, W. Roosendaal, C. Onorati, A. Sciacovelli, Y. Liu, T. Mokobodi, D. S. McGee, K.J. Craig, Initial experimental testing of a hybrid solar-dish Brayton cycle for combined heat and power (ST-CHP), Appl. Therm. Eng. 249 (2024) 1–22.

[15] Samad Power Ltd., "HIGH SPEED DIRECT DRIVE TURBOGENERATOR," Web Design & Development – 123 Internet Group, [Online]. Available: https://samad-power.co.uk/. [Accessed 16 August 2024].

[16] D.S. McGee, W.G. Le Roux, Techniques to mitigate membrane displacement for vacuum-membrane solar-dish facets, Appl. Therm. Eng. 258 (2025) 124593.

[17] Sanders Associates Inc, Parabolic dish module experiment. Final test report, Nashua, New Hampshire, USA, 1986.

[18] Garrett Turbine Engine Co., "Brayton cycle solarized advanced gas turbine: Final report," Phoenix, Arizona, USA, DOE/NASA/0181, 1986.

[19] L.D. Jaffe, Test results on parabolic dish concentrators for solar thermal power systems, Sol. Energy 42 (2) (1989) 173–187.

[20] M. Lanchi, M. Montecchi, T. Crescenzi, D. Mele, A. Miliozzi, V. Russo, D. Mazzei, M. Misceo, M. Falchetta, R. Mancini, Investigation into the coupling of micro gas turbines with CSP technology: OMSoP project, Energy Procedia 69 (2015) 1317–1326.

[21] L. Aichmayer, J. Garrido, B. Laumert, Scaling effects of a novel solar receiver for a micro gas-turbine based solar dish system, Sol. Energy 162 (2018) 248–264.

[22] W. Wang, A. Malmquist, B. Laumert, Comparison of potential control strategies for an impinging receiver based dish-Brayton system when the solar irradiation exceeds its design value, Energ. Conver. Manage. 169 (2018) 1–12.

[23] L. Aichmayer, J. Garrido, B. Laumert, Thermo-mechanical solar receiver design and validation for a micro gas-turbine based solar dish system, Energy 196 (2020).

[24] M. Lanchi, J. Al-Zaili, V. Russo, M. Falchetta, M. Montecchi, L. Aichmayer, A quasi-steady state model of a solar parabolic dish micro gas turbine demonstration plant, Energies, 15(3), (2022).

[25] J. Kesseli, E. Vollnogle, "Brayton Power Conversion System," Brayton Energy LLC, DE-FC36-08GO18029/A000, Hampton, New Hampshire, USA, 2011.

[26] H.H. Pourasl, R.V. Barenji, V.M. Khojastehnezhad, Solar energy status in the world: a comprehensive review, Energy Rep. 10 (2023) 3474–3493.

[27] A.H. Van der Merwe, W.G. Le Roux, E.D. Humphries, Parallel turbochargers for small-scale power generation, Appl. Therm. Eng. 235 (2023) 1–23.

[28] J.H. De Beer, W.G. Le Roux, A. Sciacovelli, J.P. Meyer, Effect of a novel cooling window on a recuperated solar-dish Brayton cycle, Renew. Energy 208 (2023) 465–480.

[29] W.P.J. Visser, S.A. Shakariyants, M. Oostveen, Development of a 3 kW microturbine for CHP applications, J. Eng. Gas Turbines Power 133 (4) (2011) 1–8.

[30] C.C. Cockcroft, W.G. Le Roux, The influence of applying turbine inlet air cooling to a small-scale parallel-flow Brayton cycle, Energ. Conver. Manage. 325 (2025), https://doi.org/10.1016/j.enconman.2024.119407.

[31] C. C. Cockcroft and W. G. Le Roux, "A Comparative Analysis Between Small-Scale Recuperated Parallel-Flow Brayton Cycles," Submitted to Applied Thermal Engineering on the 21st of September, 2024, Manuscript number: ATE-D-24-07833R2.

[32] I.H. Bell, J. Wronski, S. Quoilin, V. Lemort, Pure and Pseudo-pure Fluid Thermophysical Property Evaluation and the Open-Source Thermophysical Property Library CoolProp, Ind. Eng. Chem. Res. 53 (6) (2014) 2498–2508.

[33] C. Borgnakke, R.E. Sonntag, Fundamentals of Thermodynamics, 9th ed., John Wiley & Sons, Michigan, 2017.

[34] Y. A. Çengel and A. J. Ghajar, Heat and Mass Transfer Fundamentals & Applications, 6th Edition in SI Units ed., Nevada: McGraw Hill Education, 2020.

[35] Garrett Motion, "Garrett Performance Turbo," 2023. [Online]. Available: https://www.garrettmotion.com/racing-and-performance/performance-turbos/?term_id=28. [Accessed 11 May 2023].

[36] Automeris, "Extract data from charts," 2024. [Online]. Available: https://automeris.io/. [Accessed 2 August 2024].

[37] Garrett Motion, "GARRETT G42-1200 73MM," 2024. [Online]. Available: https://www.garrettmotion.com/racing-and-performance/performance-catalog/turbo/g-series-g42-1200/. [Accessed 2 August 2024].

[38] Afrox, "Section 5 - LPG," 2022. [Online]. Available: https://www.afrox.co.za/en/images/Section%205%20-%20LPG_tcm266-664444.pdf. [Accessed 7 August 2024].

[39] H. Lefebvre, D.R. Ballal, Gas Turbine Combustion: Alternative Fuels and Emissions, 3rd ed., Taylor and Francis Group, LLC, Boca Raton, 2010.

[40] G.F. Nellis, J.M. Pfotenhauer, Effectiveness-NTU relationship for a counterflow heat exchanger subjected to an external heat transfer, J. Heat Transfer 127 (2005) 1071–1073.

[41] The National Renewable Energy Laboratory, "SolTrace," [Online]. Available: https://www.nrel.gov/csp/soltrace.html. [Accessed 20 August 2024].